PHYSICAL REVIEW D **86,** 094509 (2012)

$SU(2)$ low-energy constants from mixed-action lattice QCD

S. R. Beane,[1,2] W. Detmold,[3,4] P. M. Junnarkar,[2] T. C. Luu,[5] K. Orginos,[3,4] A. Parreño,[6] M. J. Savage,[7] A. Torok,[8] and A. Walker-Loud[9,10]

(NPLQCD Collaboration)

[1]*Albert Einstein Zentrum für Fundamentale Physik, Institut für Theoretische Physik, Sidlerstrasse 5, CH-3012 Bern, Switzerland*
[2]*Department of Physics, University of New Hampshire, Durham, New Hampshire 03824-3568, USA*
[3]*Department of Physics, College of William and Mary, Williamsburg, Virginia 23187-8795, USA*
[4]*Jefferson Laboratory, 12000 Jefferson Avenue, Newport News, Virginia 23606, USA*
[5]*N Division, Lawrence Livermore National Laboratory, Livermore, California 94551, USA*
[6]*Departament d'Estructura i Constituents de la Matèria and Institut de Ciències del Cosmos, Universitat de Barcelona, E-08028 Barcelona, Catalunya, Spain*
[7]*Department of Physics, University of Washington, Seattle, Washington 98195-1560, USA*
[8]*Department of Physics, Indiana University, Bloomington, Indiana 47405, USA*
[9]*Nuclear Science Division, Lawrence Berkeley National Laboratory, Berkeley, California 94720, USA*
[10]*Department of Physics, University of California, Berkeley, California 94720, USA*

(Received 30 August 2011; published 12 November 2012)

An analysis of the pion mass and pion decay constant is performed using mixed-action lattice QCD calculations with domain-wall valence quarks on ensembles of rooted, staggered $n_f = 2 + 1$ configurations generated by the MILC Collaboration. Calculations were performed at two lattice spacings of $b \approx 0.125$ fm and $b \approx 0.09$ fm, at two strange quark masses, multiple light quark masses, and a number of lattice volumes. The ratios of light quark to strange quark masses are in the range $0.1 \leq m_l/m_s \leq 0.6$, while pion masses are in the range $235 \lesssim m_\pi \lesssim 680$ MeV. A two-flavor chiral perturbation theory analysis of the lattice QCD calculations constrains the Gasser-Leutwyler coefficients $\bar{l}_3$ and $\bar{l}_4$ to be $\bar{l}_3 = 4.04(40)(^{73}_{55})$ and $\bar{l}_4 = 4.30(51)(^{84}_{60})$. All systematic effects in the calculations are explored, including those from the finite lattice space-time volume, the finite lattice spacing, and the finite fifth dimension in the domain-wall quark action. A consistency is demonstrated between a chiral perturbation theory analysis at fixed lattice spacing combined with a leading order continuum extrapolation, and the mixed-action chiral perturbation theory analysis which explicitly includes the leading order discretization effects. Chiral corrections to the pion decay constant are found to give $f_\pi/f = 1.062(26)(^{42}_{40})$ where f is the decay constant in the chiral limit, and when combined with the experimental determination of f_π results in a value of $f = 122.8(3.0)(^{4.6}_{4.8})$ MeV. The most recent scale setting by the MILC Collaboration yields a postdiction of $f_\pi = 128.2(3.6)(^{4.4}_{6.0})(^{1.2}_{3.3})$ MeV at the physical pion mass. A detailed error analysis indicates that precise calculations at lighter pion masses is the single most important systematic to address to improve upon the present work.

DOI: 10.1103/PhysRevD.86.094509 PACS numbers: 12.38.Gc

I. INTRODUCTION

The masses and decay constants of the pseudo-Goldstone bosons are hadronic observables that lattice QCD can now calculate with percent-level accuracy in the absence of isospin breaking and electromagnetism. This is primarily due to the fact that the signal-to-noise ratio of the ground state contribution to pion correlation functions does not degrade exponentially with time. While lattice QCD calculations are still being carried out at unphysically large quark masses, with relatively coarse lattice spacings, and in modest volumes, chiral perturbation theory (χPT) can be used to describe the dependence of the pseudo-Goldstone boson masses and decay constants on these variables. Such a description involves a set of low-energy constants (LECs), which can be determined from experimental measurements, or from the lattice QCD calculations themselves. The LECs that are extracted from the pseudo-Goldstone boson observables also appear in other physical processes, and therefore accurate lattice QCD calculations of pion and kaon correlation functions are beginning to translate into predictive power for other—more complicated—observables involving pions and kaons.

χPT, the low-energy effective field theory (EFT) of QCD, provides a systematic description of low-energy processes involving the pseudo-Goldstone bosons [1]. The theory consists of an infinite series of operators (and their coefficients, the LECs) whose forms are constrained by the global symmetries of QCD. The quantitative relevance of these operators is dictated by an expansion in terms of the pion momentum and light quark masses

suppressed by the chiral symmetry breaking scale, Λ_χ. At leading order (LO) in the two-flavor ($n_f = 2$) chiral expansion, the two coefficients that appear are determined by the pion mass, m_π, and the pion decay constant, f_π. At next-to-leading order (NLO), there are four new operators in the isospin limit whose coefficients are not constrained by global symmetries [2]; these LECs are the Gasser-Leutwyler coefficients. Two of these LECs, $\bar{l}_1$ and $\bar{l}_2$, can be reliably determined from low-energy $\pi\pi$ scattering [3]. The LEC $\bar{l}_3$ governs the size of the NLO contributions to m_π, while $\bar{l}_4$ controls the size of the NLO contributions to f_π. Lattice QCD, the numerical solution of QCD, provides a way to constrain these coefficients, including those that depend upon the light quark masses. Further, as lattice QCD calculations can be performed to arbitrary precision with appropriate computational resources, they will likely provide more precise determinations of the LECs than can be extracted from experimental data. A number of lattice collaborations have recently determined $\bar{l}_3$ and $\bar{l}_4$ using $n_f = 2$, $n_f = 2 + 1$ and $n_f = 2 + 1 + 1$ calculations of m_π and f_π with a variety of lattice discretizations [4–11]. These efforts have been compiled into a review article [12] which has performed averages of these various computational efforts. It should be noted that there is an increasing number of lattice QCD calculations performed at or near the physical point [6,13–16], and it will be exciting to have reliable predictions of hadronic observables that do not rely on χPT.

In this work, we focus on the determination of $\bar{l}_3$ and $\bar{l}_4$ from the pion mass and the pion decay constant using a mixed-action (MA) calculation with domain-wall valence quarks on gauge-field configurations generated with rooted, staggered sea quarks. This serves to strengthen the case that the systematic effects arising from the finite lattice spacing, which are unique to a given lattice discretization, can be systematically eliminated to produce results that are independent of the fermion and gauge lattice actions. There are already preliminary results from mixed-action calculations which can be found in Ref. [17].

Section II describes the details of the lattice QCD calculation. In Sec. III, details of the systematic uncertainties are presented. Continuum and chiral extrapolations of the results of the lattice QCD calculations are detailed in Sec. IV. Conclusions are presented in Sec. V.

II. DETAILS OF THE LATTICE CALCULATION AND NUMERICAL DATA

The present work is part of a program of mixed-action lattice QCD calculations performed by the NPLQCD Collaboration [18–32]. The strategy, initiated by the LHP Collaboration [33–38], is to compute domain-wall fermion [39–43] propagators generated on the $n_f = 2 + 1$ asqtad-improved [44,45] rooted, staggered sea-quark configurations generated by the MILC Collaboration [46,47] (with hypercubic-smeared [48–51] gauge links to improve the chiral symmetry properties of the domain-wall propagators). The predominant reason for the success of this program is the good chiral symmetry properties of the domain-wall action, which significantly suppresses chiral symmetry breaking from the staggered sea fermions and discretization effects [52–54]. This particular mixed-action approach has been used to perform a detailed study of the meson and baryon spectrum [37] including a comparison with predictions from the large-N_c limit of QCD and $SU(3)$ chiral symmetry [55,56]. The static and charmed baryon spectrum were, respectively, determined in Refs. [57,58]; the first calculation of the hyperon axial charges was performed in Ref. [59]; the first calculation of the strong isospin breaking contribution to the neutron-proton mass difference was calculated in Ref. [21], and the hyperon electromagnetic form factors were explored in Ref. [60]. The majority of calculations using this mixed-action strategy have been performed at only one lattice spacing, the *coarse* lattice spacing of $b \approx 0.125$ fm; a notable exception was the calculation of B_K [61], which included the *fine* MILC ensembles with $b \approx 0.09$ fm. In Ref. [62], very nice agreement was found between the prediction of the scalar a_0 correlation function from mixed-action χPT (MAχPT) and the lattice QCD calculations of the same correlation function [63]. This was an important check of the understanding of unitarity violations that are inherent in mixed-action calculations.

A. Lattice QCD parameters

In our previous works [18–32], on the $b \approx 0.125$ fm ensembles, domain-wall valence propagators were calculated on half the time extent of the MILC lattices by using a Dirichlet boundary condition (BC) in the time direction. With the relatively high statistics that have now been accumulated, systematic effects from the light states reflecting off the Dirichlet wall are observed and are found to contaminate the correlation functions in the region of interest (see Fig. 1). This ''lattice chopping'' strategy has been discarded, and the valence propagators are now calculated with antiperiodic temporal BCs imposed at the end of the full time extent of each configuration. The exception is on the heaviest light quark mass point of the $b \approx 0.125$ fm ensemble. At this heavy pion mass, the correlation function falls sufficiently rapidly to not be significantly impacted in the region of interest by the choice of BC. Further, this ensemble contributes very little to our analysis in Sec. IV.

The parameters used in the present set of lattice QCD calculations are presented in Table I. On the $b \approx 0.125$ fm configurations, light quark propagators computed by LHPC with antiperiodic temporal BCs are used for the three lightest ensembles [38]. Strange quark propagators are computed from the same source points in order to ''match'' the light quark propagators. In addition, calculations on the $b \approx 0.125$ fm ensembles with a lighter than

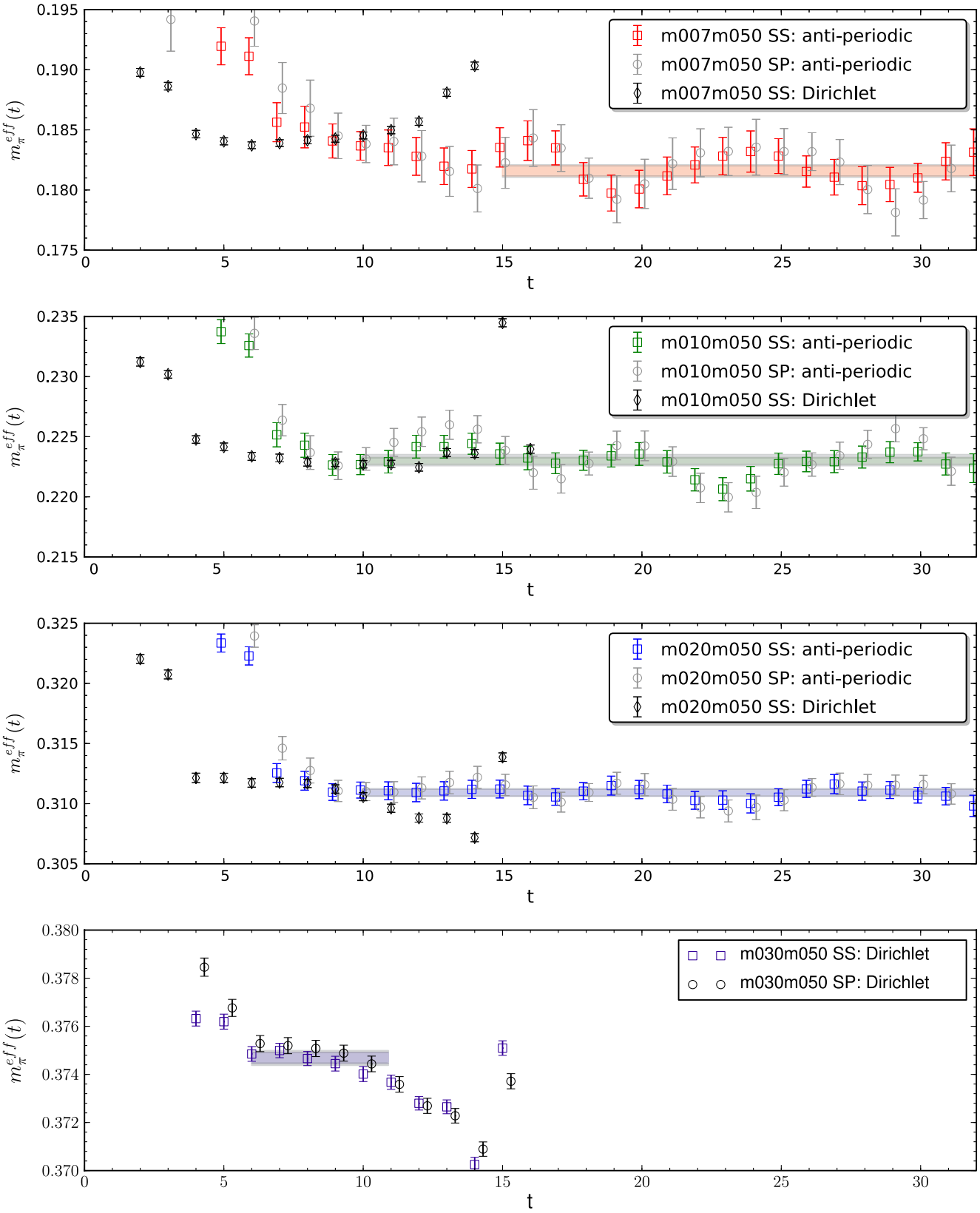

FIG. 1 (color online). EMPs of the pion correlation functions on the $b \approx 0.125$ fm ensembles. For comparative purposes, the effective masses from the correlation functions with Dirichlet BCs in time are shown for the lightest ensembles (slightly offset for visibility).

TABLE I. The parameters used in the lattice QCD calculations.

$b \approx 0.125$ fm ensembles											
β	bm_l^{sea}	bm_s^{sea}	L	T	M_5	L_5	bm_l^{dwf}	bm_l^{res}	bm_s^{dwf}	bm_s^{res}	$N_{\text{src}} \times N_{\text{cfg}}$
6.76	0.007	0.050	20	64	1.7	16	0.0081	0.001581(14)[a]	0.081	0.000895(3)	4×468
6.76	0.007	0.050	24	64	1.7	16	0.0081	0.00164(3)	0.081	0.00091(2)	8×1081
6.76	0.010	0.050	20	64	1.7	16	0.0138	0.001566(11)[a]	0.081	0.000913(2)	4×656
6.76	0.010	0.050	28	64	1.7	16	0.0138	0.001566(11)[a]	0.081	0.000913(2)	4×274
6.79	0.020	0.050	20	64	1.7	16	0.0313	0.001227(11)[a]	0.081	0.000836(3)	4×486
6.81	0.030	0.050	20	32	1.7	16	0.0478	0.001013(6)	0.081	0.000862(7)	24×564
$b \approx 0.09$ fm ensembles											
β	bm_l^{sea}	bm_s^{sea}	L	T	M_5	L_5	bm_l^{dwf}	bm_l^{res}	bm_s^{dwf}	bm_s^{res}	$N_{\text{src}} \times N_{\text{cfg}}$
7.08	0.0031	0.031	40	96	1.5	40	0.0038	0.000156(3)	0.0423	0.000073(2)	1×170
7.08	0.0031	0.031	40	96	1.5	12	0.0035	0.000428(3)	0.0423	0.000233(2)	1×422
7.09	0.0062	0.031	28	96	1.5	12	0.0080	0.000375(4)	0.0423	0.000230(3)	7×1001
7.11	0.0124	0.031	28	96	1.5	12	0.0164	0.000290(3)	0.0423	0.000204(2)	8×513

[a]Provided by LHPC [38].

physical strange quark mass have been performed. Statistics on three $b \approx 0.09$ fm ensembles have been accumulated, with the lightest pion mass being $m_\pi \approx 235$ MeV. Finally, approximately 6500 thermalized trajectories have been completed on an additional rooted staggered ensemble with the parameters

$$\beta = 6.76, \qquad bm_l^{\text{sea}} = 0.007, \qquad bm_s^{\text{sea}} = 0.050, \qquad V = 24^3 \times 64, \tag{1}$$

and measurements have been performed on them.

B. Results of the lattice QCD calculations

Correlation functions with the quantum numbers of the π^+ were constructed from propagators generated from a gauge-invariant Gaussian-smeared source [64,65] with both smeared (SS) and point (SP) sinks. To determine the pion mass, the correlation functions were fit with a single cosh toward the center of the time direction.

$$C_{(SX)}(t) \sim A_{(SX)} e^{-m_\pi T/2} \cosh(m_\pi (t - T/2)), \tag{2}$$

where $X = S, P$. Fits incorporating excited states over larger time ranges produced consistent results for both m_π and $A_{(SX)}$. With domain-wall fermions, the pion decay constant can be computed without need for operator renormalization by making use of an axial ward identity [66]. The decay constant is determined from the extracted overlap factors, $A_{(SX)}$, along with the input quark masses and computed values of the pion mass and residual mass, using the relation

$$bf_\pi = \frac{A_{SP}}{\sqrt{A_{SS}}} \frac{2\sqrt{2}(bm_l^{\text{dwf}} + bm_l^{\text{res}})}{(bm_\pi)^{3/2}}. \tag{3}$$

TABLE II. The pion masses and decay constants from the lattice QCD calculations. The first uncertainty is statistical and the second is systematic determined from the fit range.

m_{sea}	$L^3 \times T_{\text{val}} \times L_5$	bm_π	bf_π	$bm_{\pi_{\text{Mix}}}$	$m_\pi L$
m007m050	$20^3 \times 64 \times 16$	$0.18159(42)(^{27}_{32})$	$0.09293(45)(^{41}_{86})$	0.2553(15)	3.63
m010m050	$20^3 \times 64 \times 16$	$0.22298(26)(^{46}_{29})$	$0.09597(27)(^{79}_{47})$	0.2842(15)	4.46
m020m050	$20^3 \times 64 \times 16$	$0.31091(27)(^{20}_{10})$	$0.10204(26)(^{33}_{21})$	0.3516(09)	6.22
m030m050	$20^3 \times 32 \times 16$	$0.37469(22)(^{20}_{22})$	$0.10749(13)(^{33}_{33})$	0.412(4)	7.49
m007m050	$24^3 \times 64 \times 16$	$0.18167(23)(^{66}_{63})$	$0.09311(28)(^{34}_{45})$	0.2553(15)	4.36
m010m050	$28^3 \times 64 \times 16$	$0.22279(21)(^{19}_{16})$	$0.09639(41)(^{50}_{37})$	0.2842(15)	6.24
m0031m031	$40^3 \times 96 \times 40$	$0.10328(32)(^{36}_{40})$	$0.0621(12)(^{10}_{13})$	0.1344(14)	4.13
m0031m031	$40^3 \times 96 \times 12$	$0.10160(22)(^{21}_{24})$	$0.0617(09)(^{10}_{13})$	0.1293(08)	4.06
m0062m031	$28^3 \times 96 \times 12$	$0.14530(15)(^{15}_{09})$	$0.06539(14)(^{34}_{30})$	0.1632(10)	4.07
m0124m031	$28^3 \times 96 \times 12$	$0.20043(17)(^{13}_{10})$	$0.07032(19)(^{20}_{40})$	0.2153(03)	5.61

In the limit $L_5 \longrightarrow \infty$, the residual chiral symmetry breaking in the domain-wall action vanishes and $m_l^{\rm res} \longrightarrow 0$. In addition to these valence quantities, the mixed valence-sea pion correlation functions have been calculated to extract the mixed-meson masses, as described in Ref. [67].

The results of the lattice QCD calculations are given in Table II. Statistical uncertainties are determined from a correlated χ^2 analysis as well as from a single-elimination jackknife. Binning of the data was performed until the uncertainties did not change appreciably. The quoted fitting systematic uncertainties are determined by varying the fit range, including a broad sweep of $t_{\rm min}$. Effective mass plots (EMPs) for the full-volume correlation functions are generated with a cosh-style effective mass;

$$m_\pi^{\rm eff} = \frac{1}{\tau}\cosh^{-1}\left[\frac{C(t+\tau)+C(t-\tau)}{2C(t)}\right], \tag{4}$$

while the others were generated with a log-style effective mass;

$$m_\pi^{\rm eff} = \frac{1}{\tau}\ln\left(\frac{C(t)}{C(t+\tau)}\right). \tag{5}$$

In Figs. 1–3 the EMPs of the correlation functions and the extracted pion masses are presented using $\tau = 3$.

In Fig. 1, the effective masses from calculations with antiperiodic BCs imposed on the valence quarks, as well as those from the Dirichlet temporal BCs, are shown. Correlation functions from propagators generated with a Dirichlet BC (located at $t = 22$ and $t = -10$ in the figures) show a significantly different behavior from those generated with antiperiodic BCs. It is for this reason that we have abandoned the Dirichlet BC in the generation of valence quarks. However, it is only the lightest ensemble on which the extracted pion mass determined with the Dirichlet BC is statistically discrepant from that generated with antiperiodic BCs.

Interestingly, the correlation functions generated with antiperiodic BCs are not free of their own systematics. The EMPs exhibit an oscillation with a period of approximately 1 fm, which is not simply explained by either the staggered taste-pion mass splittings or by the mixed-meson mass splittings. In the top panel of Fig. 2, the oscillations are more pronounced (with higher statistics). Comparing the EMPs from the $b \approx 0.09$ fm and $b \approx 0.125$ fm ensembles, the oscillations are seen to become more pronounced for lighter quark masses. As the statistics are increased, the amplitude of the oscillation becomes more significant and increasing L_5 does not appear to ameliorate these effects. The choice of τ used in Eq. (4) has no appreciable impact on the observed oscillation, unless one takes $\tau \simeq T_{\rm osc}$, the oscillation period, in which case the oscillations are washed out. At this point, it is not clear if the oscillations

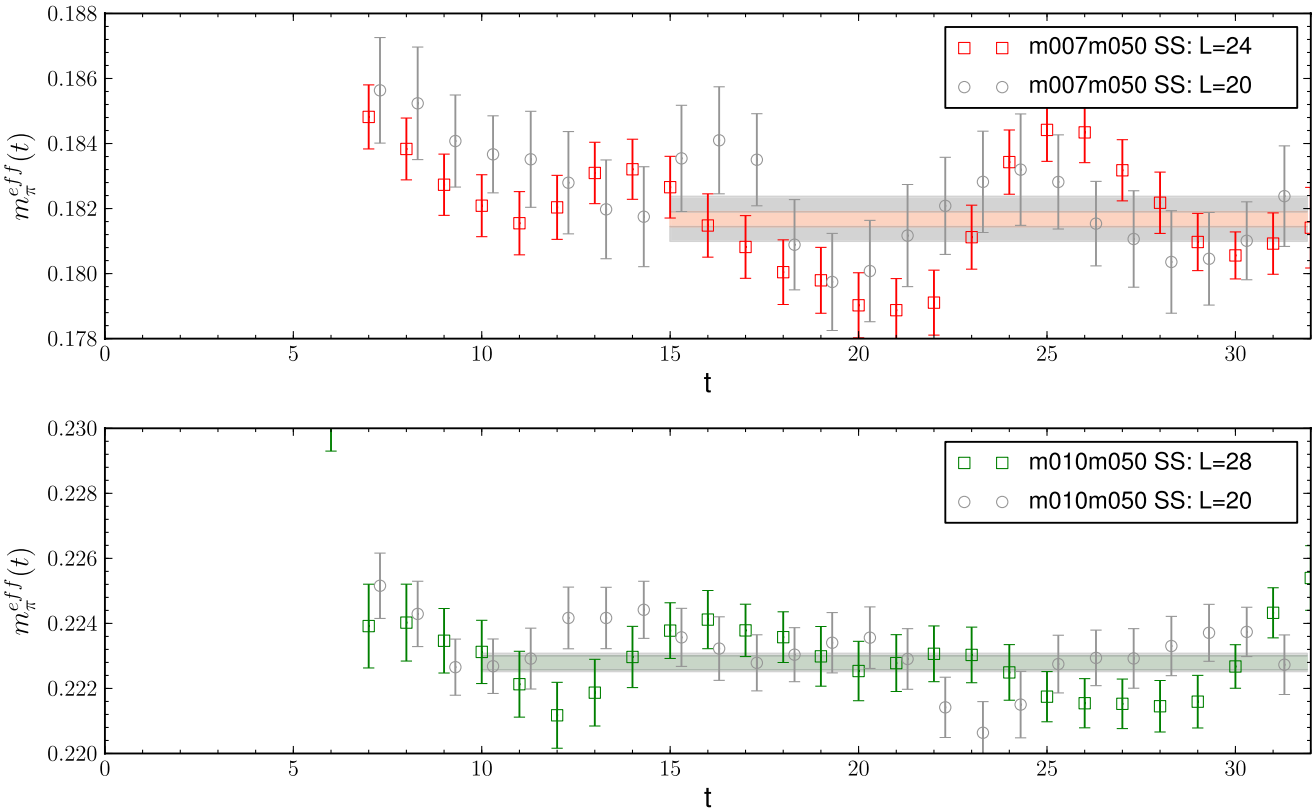

FIG. 2 (color online). EMPs of the pion correlation functions calculated on the large volume $b \approx 0.125$ fm ensembles. For comparative purposes, the effective masses obtained in the smaller volumes are shown (slightly offset in time for visibility).

are an artifact of this particular mixed action or originate from the domain-wall valence propagators. Similar oscillations are observed for calculations with domain-wall valence propagators computed on dynamical domain-wall ensembles, as shown in Fig. 11 of Ref. [9] and Fig. 2 of Ref. [68]. In Ref. [69], it was suggested that these fluctuations may be explained by the time correlations in the propagators. However, in Refs. [70–73], a calculation of

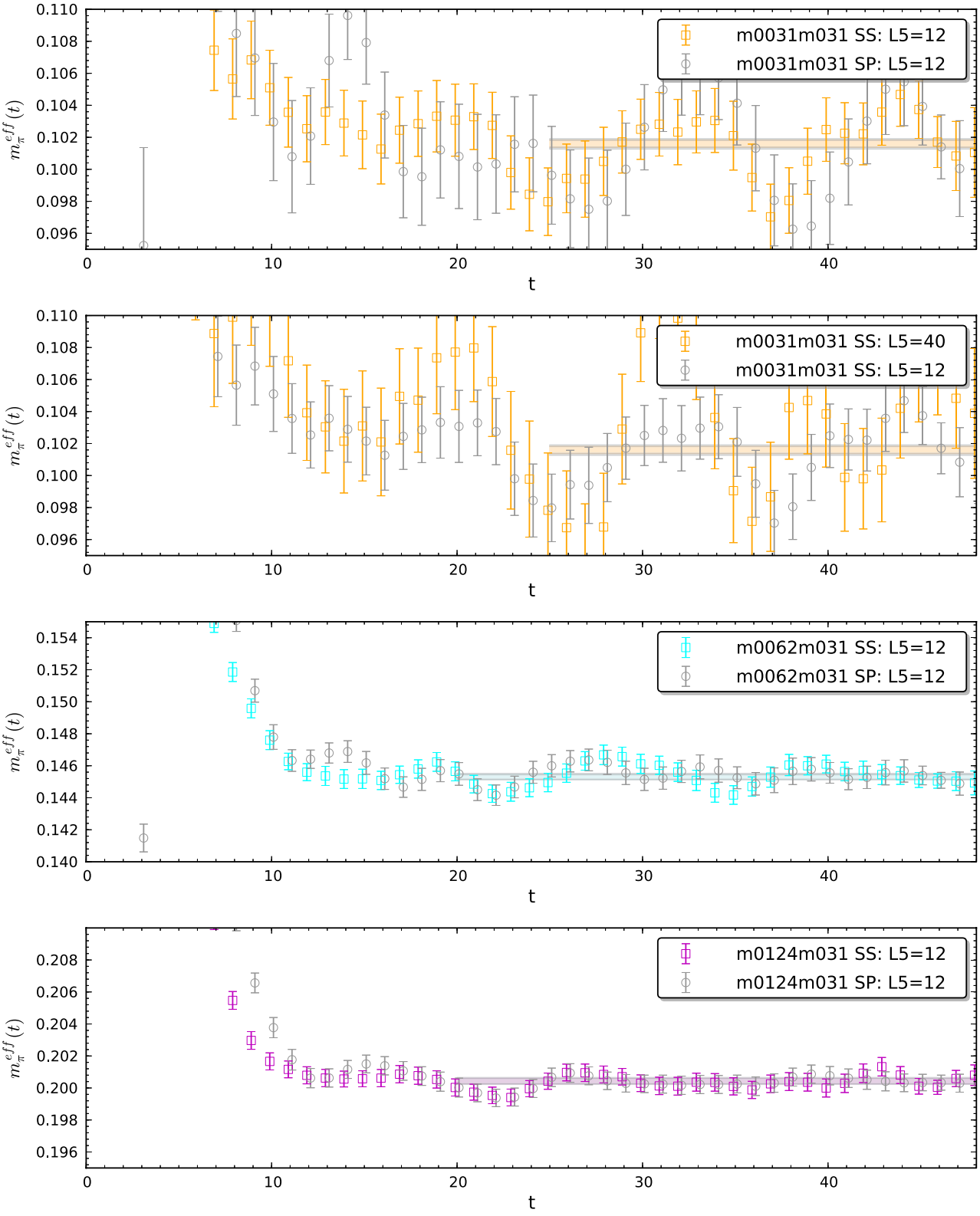

FIG. 3 (color online). EMPs of the pion correlation functions on the $b \approx 0.09$ fm ensembles.

TABLE III. The pion masses (normalized to the light quark masses) and decay constants in r_1 units. The third uncertainty is the systematic from the conversion to r_1 units.

Ensemble masses	V	$\frac{(r_1 m_\pi)^2}{r_1 m_q}$	$r_1 f_\pi$
m007m050	$20^3 \times 64 \times 16$	$9.310(43)(^{26}_{31})(11)$	$0.2545(12)(^{11}_{23})(03)$
m010m050	$20^3 \times 64 \times 16$	$8.861(21)(^{37}_{23})(10)$	$0.2628(08)(^{23}_{14})(03)$
m020m050	$20^3 \times 64 \times 16$	$8.384(14)(^{10}_{05})(10)$	$0.2879(07)(^{09}_{06})(03)$
m030m050	$20^3 \times 32 \times 16$	$8.275(10)(^{09}_{10})(12)$	0.3093(04)(10)(05)
m007m050	$24^3 \times 64 \times 16$	$9.318(23)(^{68}_{63})(11)$	$0.2550(08)(^{10}_{13})(03)$
m010m050	$28^3 \times 64 \times 16$	$8.846(16)(^{14}_{12})(10)$	$0.2640(11)(^{12}_{10})(03)$
m0031m031	$40^3 \times 96 \times 40$	$10.123(62)(^{70}_{78})(11)$	$0.2331(45)(^{38}_{49})(03)$
m0031m031	$40^3 \times 96 \times 12$	$9.942(57)(^{54}_{62})(11)$	$0.2318(34)(^{38}_{49})(03)$
m0062m031	$28^3 \times 96 \times 12$	$9.551(20)(^{20}_{12})(08)$	$0.2477(05)(^{12}_{11})(02)$
m0124m031	$28^3 \times 96 \times 12$	$9.285(16)(^{12}_{09})(10)$	$0.2713(07)(^{07}_{15})(03)$

TABLE IV. r_1/b from MILC [47]. The values (provided by the MILC Collaboration) extrapolated to the physical light quark masses (rightmost column) were used to convert from lattice units to r_1 units.

Ensemble masses	β	$\frac{r_1}{b}(bm_l, bm_s, \beta)$	$\frac{r_1}{b}(bm_l^{\rm phy}, bm_s^{\rm phy}, \beta)$
m007m050	6.76	2.635(3)	2.739(3)
m010m050	6.76	2.618(3)	2.739(3)
m020m050	6.79	2.644(3)	2.821(3)
m030m050	6.81	2.650(4)	2.877(4)
m0031m031	7.08	3.695(4)	3.755(4)
m0062m031	7.09	3.699(3)	3.789(3)
m0124m031	7.11	3.712(4)	3.858(4)

the pion correlation function was performed with ~400 times the number of measurements analyzed in Ref. [69], and no evidence for such oscillations or fluctuations was found (see Figs. 17 and 18 of Ref. [73]). For the present work, the masses and decay constants are determined with fits that encompass at least one full period of oscillation, with the fitting systematic established through variations of the fitting ranges.

C. Scale setting

To extrapolate the calculated pion masses and decay constants and make predictions at the physical pion mass, the scale must be determined. The MILC Collaboration has performed extensive scale setting analyses on their ensembles, and it is used to convert the calculated pion masses and decay constants into r_1 units (extrapolated to the physical values of the light quark masses),[1] collected in Table III. In Table IV these values are listed for the ensembles used in this work [47]. The MILC Collaboration has determined $r_1 = 0.318(7)$ fm using the $b\bar{b}$ meson spectrum and $r_1 = 0.311(2)(^{3}_{8})$ fm using f_π to set the scale [47]. The value of

$$r_1 = 0.311(2)(^{3}_{8})\ \text{fm} \tag{6}$$

is used in this work to convert to physical units.

[1]The distance r_1 is the Sommer scale [74] defined from the heavy-quark potential at the separation, $r_1^2 F(r_1) \equiv -1$.

III. LATTICE SYSTEMATICS

In order to make contact with experimental measurements, the lattice QCD results must be extrapolated to the continuum and to infinite volume, as well as to the physical values of the light quark masses. χPT is the natural tool to perform these extrapolations, a consequence of which is that the LECs can be determined.

A. Light quark mass and volume dependence

Generally, the chiral expansion at NLO involves analytic terms, chiral logarithms and scale-dependent LECs. However, the perturbative expansion can be optimized by setting the renormalization scale to lattice-determined quantities which vary with the quark mass, leading to modifications at next-to-next-to-leading order (NNLO). For instance, the $SU(2)$ chiral expansion of m_π and f_π can be expressed as [12,18]

$$m_\pi^2 = 2Bm_q\left\{1 + \frac{1}{2}\xi \ln\left(\frac{\xi}{\xi^{\rm phy}}\right) - \frac{1}{2}\xi \bar{l}_3\right\}, \tag{7}$$

$$f_\pi = f\left\{1 - \xi \ln\left(\frac{\xi}{\xi^{\rm phy}}\right) + \xi \bar{l}_4\right\}, \tag{8}$$

where

$$\xi = \frac{m_\pi^2}{8\pi^2 f_\pi^2} \quad \text{and} \quad \bar{l}_i = \log\frac{\Lambda_i^2}{(m_\pi^{\rm phy})^2}, \tag{9}$$

and Λ_i is an intrinsic scale that is not determined by chiral symmetry. Here m_π and f_π denote lattice-measured quantities, f is the chiral-limit value of the pion decay constant, and B is proportional to the chiral condensate. The "phy" superscript indicates that the relevant quantity is evaluated with the physical values of the pion mass and decay constant, for which we use the central values

$$f_\pi^{\rm phy} = 130.4 \text{ MeV} \quad \text{and} \quad m_\pi^{\rm phy} = 139.6 \text{ MeV}. \tag{10}$$

One benefit of performing the perturbative expansion with ξ is immediately clear: as ξ is dimensionless, the higher order corrections are free of scale setting ambiguities as only the LO order contributions must be expressed in terms of some lattice scale.

In addition to the light quark mass dependence, the finite-volume corrections to the pion masses and decay constants can be simply determined in the p regime, defined by $m_\pi L \gg 1$. At NLO in the chiral expansion, the finite-volume corrections are given by [75,76]

$$\Delta^{(\rm FV)}\frac{m_\pi^2}{2Bm_q} = 8\pi^2\Delta i\mathcal{I}(\xi, m_\pi L), \tag{11}$$

$$\Delta^{(\rm FV)}\frac{f_\pi}{f} = -16\pi^2\Delta i\mathcal{I}(\xi, m_\pi L), \tag{12}$$

where

$$8\pi^2\Delta i\mathcal{I}(\xi, m_\pi L) = \frac{2\xi}{m_\pi L}\sum_{n=1}^{\infty}\frac{k(n)}{\sqrt{n}}K_1(\sqrt{n}m_\pi L) \tag{13}$$

and $k(n)$ is the number of ways that the integer n can be formed as the sum of squares of three integers, $n = \sum_{i=1}^3 n_i^2$ with $n_i \in \mathbb{Z}$.

The light quark mass dependences of m_π and f_π are known at NNLO in two-flavor χPT [77]. In the ξ expansion, in infinite volume, they are

$$\begin{aligned}\frac{m_\pi^2}{2Bm_q} &= 1 + \frac{1}{2}\xi\left[\ln\left(\frac{\xi}{\xi^{\rm phy}}\right) - \bar{l}_3\right] + \frac{7}{8}\xi^2\ln^2(\xi) \\ &\quad - \left[\frac{16}{3} + \frac{1}{3}\bar{l}_{12} - \frac{9}{4}\bar{l}_3 - \bar{l}_4 - \frac{7}{4}\ln(\xi^{\rm phy})\right]\xi^2\ln(\xi) \\ &\quad - \bar{l}_4\xi\xi^{\rm phy} + \xi^2 k_M\end{aligned} \tag{14}$$

and

$$\begin{aligned}\frac{f_\pi}{f} &= 1 + \xi\left[\bar{l}_4 - \ln\left(\frac{\xi}{\xi^{\rm phy}}\right)\right] + \frac{5}{4}\xi^2\ln^2(\xi) \\ &\quad + \xi^2\ln(\xi)\left[\frac{53}{12} + \frac{1}{6}\bar{l}_{12} - 5\bar{l}_4 - \frac{5}{2}\ln(\xi^{\rm phy})\right] \\ &\quad + 2\bar{l}_4\xi\xi^{\rm phy} + \xi^2 k_F,\end{aligned} \tag{15}$$

where $\bar{l}_{12} = 7\bar{l}_1 + 8\bar{l}_2$.

B. Mixed-action χPT

The low-energy EFT for mixed-action lattice QCD calculations is well understood [52–54,62,63,67,78–85]. In Refs. [53,54,85], it was demonstrated that the formulas for the pion mass and decay constant at NLO, including discretization effects, are the same for all sea-quark discretizations provided the valence quarks satisfy the Ginsparg-Wilson relation [86] (including our MA approach with domain-wall valence propagators computed on rooted staggered sea-quark configurations). The difference between the various sea-quark actions will be encoded in the values of the unphysical parameters which quantify the discretization effects. At NLO in the MA expansion, including finite-volume effects, the pion mass and decay constant are given by

$$\begin{aligned}\frac{m_\pi^2}{2Bm_q} &= 1 + \frac{1}{2}\xi\ln\left(\frac{\xi}{\xi^{\rm phy}}\right) - \frac{1}{2}\xi\bar{l}_3 \\ &\quad - \frac{1}{2}(\tilde{\xi}_{\rm sea} - \xi)[1 + \ln(\xi)] - l_3^{\rm PQ}(\xi_{\rm sea} - \xi) \\ &\quad + l_3^b\left(\frac{b}{r_1}\right)^2 + 8\pi^2\Delta i\mathcal{I}(\xi, m_\pi L) \\ &\quad + 8\pi^2(\tilde{\xi}_{\rm sea} - \xi)\Delta\partial i\mathcal{I}(m_\pi L),\end{aligned} \tag{16}$$

$$\begin{aligned}\frac{f_\pi}{f} &= 1 - \tilde{\xi}_{\rm Mix}\ln\left(\frac{\tilde{\xi}_{\rm Mix}}{\xi^{\rm phy}}\right) + \xi\bar{l}_4 - (\tilde{\xi}_{\rm Mix} - \xi)\ln(\xi^{\rm phy}) \\ &\quad - l_4^{\rm PQ}(\xi_{\rm sea} - \xi) + l_4^b\left(\frac{b}{r_1}\right)^2 - 16\pi^2\Delta i\mathcal{I}(\tilde{\xi}_{\rm Mix}, m_{\pi_{\rm Mix}}L),\end{aligned} \tag{17}$$

where

$$\begin{aligned}\Delta\partial i\mathcal{I}(mL) &= \frac{1}{(4\pi)^2}\sum_{n=1}^{\infty}k(n)\Big(K_0(\sqrt{n}mL) + K_2(\sqrt{n}mL) \\ &\quad - \frac{2K_1(\sqrt{n}mL)}{\sqrt{n}mL}\Big).\end{aligned} \tag{18}$$

For the present calculations, the extra expansion parameters of the theory are defined as

$$\begin{aligned}\tilde{\xi}_{\rm Mix} &= \frac{\frac{1}{2}(m_\pi^2 + m_{\pi_{\rm sea,5}}^2) + b^2\Delta'_{\rm Mix}}{8\pi^2 f_\pi^2}, \\ \tilde{\xi}_{\rm sea} &= \frac{m_{\pi_{\rm sea,5}}^2 + b^2\Delta_{\rm I}}{8\pi^2 f_\pi^2}, \qquad \xi_{\rm sea} = \frac{m_{\pi_{\rm sea,5}}^2}{8\pi^2 f_\pi^2},\end{aligned} \tag{19}$$

where $m_{\pi_{\rm sea,5}}$ is the taste-5 staggered pion mass, $b^2\Delta_{\rm I}$ is the mass splitting of the taste identity staggered pion and $b^2\Delta'_{\rm Mix}$ is the mass splitting of the mixed valence-sea pion [80,85], determined in Refs. [62,67] and this work. In Table V, the values of the parameters relevant for the calculations are listed.

In analogy with finite-volume χPT, the pion mass and pion decay constant in finite-volume MAχPT are related to their infinite-volume values at NLO via the relations

TABLE V. Expansion parameters m_l/m_s, ξ, $\tilde{\xi}_{\rm Mix}$, $\tilde{\xi}_{\rm sea}-\xi$, $\xi_{\rm sea}-\xi$ and $\frac{m^{\rm res}}{m_q}$.

$m_{\rm sea}$	V	m_l/m_s	ξ	$\tilde{\xi}_{\rm Mix}$	$\tilde{\xi}_{\rm sea}-\xi$	$\xi_{\rm sea}-\xi$	$\frac{m^{\rm res}}{m_q}$
m007m050	$20^3\times 64\times 16$	0.14	0.0491	0.096	0.114	0.0032	0.165
m010m050	$20^3\times 64\times 16$	0.20	0.0681	0.111	0.108	0.0010	0.102
m020m050	$20^3\times 64\times 16$	0.40	0.1177	0.150	0.093	0.0001	0.038
m030m050	$20^3\times 32\times 16$	0.60	0.1540	0.186	0.084	0.0026	0.021
m007m050	$24^3\times 64\times 16$	0.14	0.0489	0.096	0.114	0.0032	0.165
m010m050	$28^3\times 64\times 16$	0.20	0.0674	0.111	0.108	0.0010	0.102
m0031m031	$40^3\times 96\times 40$	0.10	0.0360	0.058	0.050	0.0004	0.039
m0031m031	$40^3\times 96\times 12$	0.10	0.0365	0.058	0.050	0.0004	0.109
m0062m031	$28^3\times 96\times 12$	0.20	0.0629	0.079	0.045	0.0019	0.045
m0124m031	$28^3\times 96\times 12$	0.40	0.1037	0.119	0.038	0.0054	0.017

$$m_\pi[\mathrm{FV}] = m_\pi\Bigg\{1+\frac{1}{2}\sum_{n=1}^{\infty}\frac{k(n)}{2}\Bigg[4\xi\frac{K_1(\sqrt{n}m_\pi L)}{\sqrt{n}m_\pi L} + (\xi_{\rm sea}-\xi)\Big(K_0(\sqrt{n}m_\pi L)+K_2(\sqrt{n}m_\pi L) - 2\frac{K_1(\sqrt{n}m_\pi L)}{\sqrt{n}m_\pi L}\Big)\Bigg]\Bigg\}, \tag{20}$$

and

$$f_\pi[\mathrm{FV}] = f_\pi\Bigg[1-4\xi_{\rm Mix}\sum_{n=1}^{\infty}k(n)\frac{K_1(\sqrt{n}m_{\pi_{\rm Mix}}L)}{\sqrt{n}m_{\pi_{\rm Mix}}L}\Bigg]. \tag{21}$$

In the case of f_π, the finite-volume effects in MAχPT are somewhat suppressed compared to those in χPT. This is because the contribution from the "average" valence-sea-type virtual pion in a one-loop diagram is smaller than from a valence-valence pion due to its larger mass [67]. In contrast, the pion mass receives a one-loop contribution from a hairpin diagram [87], which has enhanced volume effects compared to a typical one-loop contribution. In Table VI, the FV contributions to m_π and f_π from Eqs. (20) and (21) are presented. On the lightest two coarse ensembles, the NLO volume contributions to m_π from MAχPT are substantially larger than those from χPT. Further, due to the high precision of the lattice QCD calculations, the finite-volume contributions are larger than the uncertainties on the m007m050 ensembles. This is in contrast to the results of the lattice QCD calculations of m_π, which show little volume dependence. In Ref. [88], it was demonstrated that NNLO χPT could increase the finite-volume contributions by as much as $\sim$50% of the NLO contribution. In the case of MAχPT, with hairpin diagrams having enhanced volume effects, the importance of the NNLO contributions is likely to be even greater than in χPT. As these NNLO effects have not yet been calculated, the MAχPT finite-volume contributions are assigned a 30% systematic uncertainty when performing the analysis in Sec. IV. In Fig. 4, the NLO finite-volume contributions in χPT and in MAχPT for the m007m050 and m010m050 ensembles are compared with the results of the lattice QCD calculations. The χPT band is given by the range $\Delta m_\pi = (1+0.5)\Delta m_\pi^{\chi\rm PT}$, while the MA$\chi$PT

TABLE VI. Finite-volume corrections to m_π and f_π at NLO in MAχPT, as given in Eqs. (20) and (21). For a quantity Y in the table, $\delta Y[\mathrm{FV}]/Y = (Y[\mathrm{FV}]-Y)/Y$.

			$b\approx 0.125$ fm ensemble			
	m007m050		m010m050		m020m050	m030m050
Quantity	$L=20$	$L=24$	$L=20$	$L=28$	$L=20$	$L=20$
MAχPT: $\delta m_\pi[\mathrm{FV}]/m_\pi$	1.6%	0.6%	0.6%	0.1%	0.1%	0.0%
χPT: $\delta m_\pi[\mathrm{FV}]/m_\pi$	0.2%	0.1%	0.1%	0.0%	0.0%	0.0%
MAχPT: $\delta f_\pi[\mathrm{FV}]/f_\pi$	−0.3%	−0.1%	−0.2%	−0.0%	−0.1%	−0.0%
χPT: $\delta f_\pi[\mathrm{FV}]/f_\pi$	−1.4%	−0.5%	−0.6%	−0.1%	−0.1%	−0.0%
			$b\approx 0.09$ fm ensemble			
	m0031m031		m0062m031		m0124m031	
Quantity	$L=40$		$L=28$		$L=28$	
MAχPT: $\delta m_\pi[\mathrm{FV}]/m_\pi$	0.4%		0.4%		0.1%	
χPT: $\delta m_\pi[\mathrm{FV}]/m_\pi$	0.1%		0.1%		0.0%	
MAχPT: $\delta f_\pi[\mathrm{FV}]/f_\pi$	−0.2%		−0.6%		−0.1%	
χPT: $\delta f_\pi[\mathrm{FV}]/f_\pi$	−0.6%		−0.9%		−0.2%	

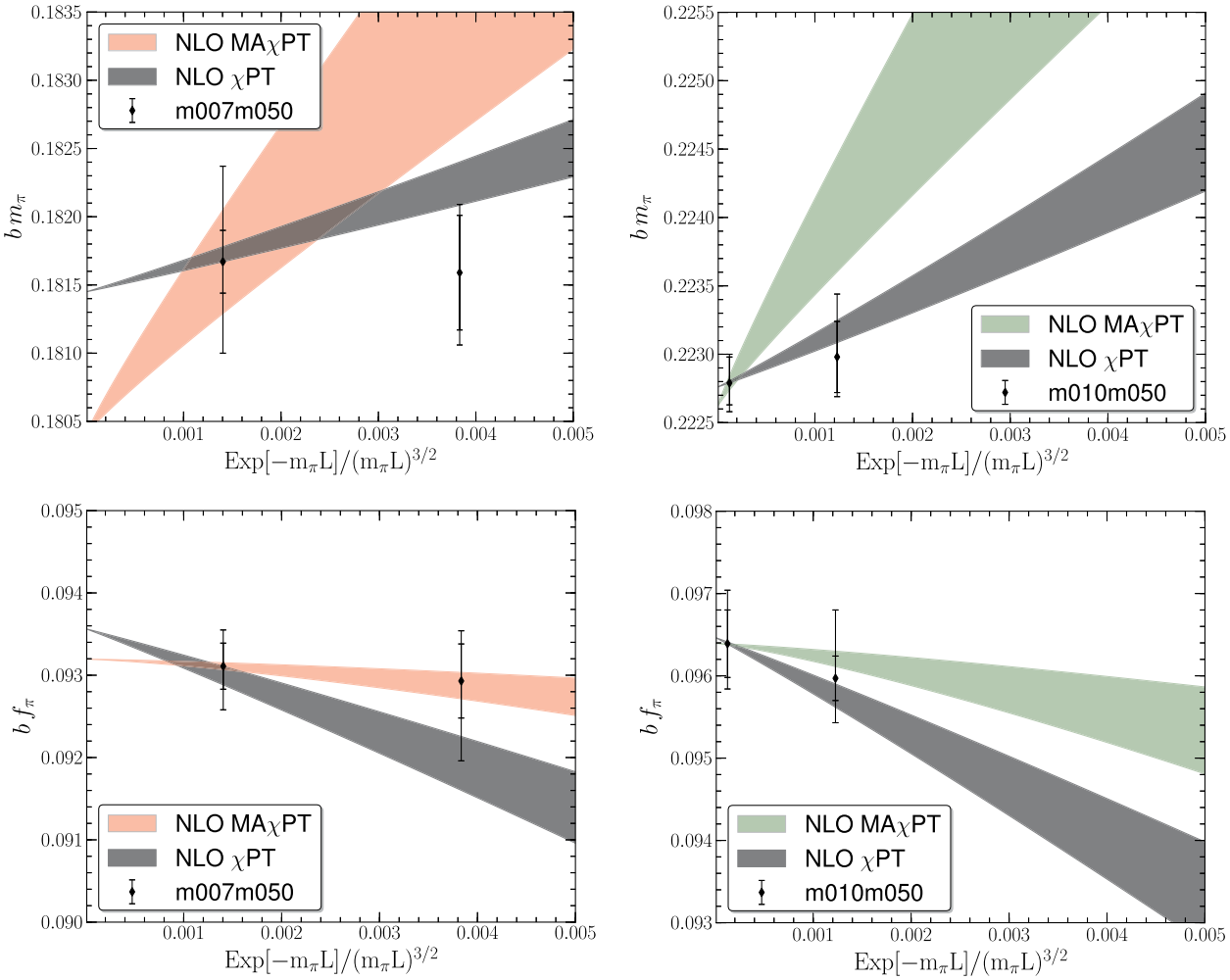

FIG. 4 (color online). NLO finite-volume contributions, and an estimate of their uncertainty, in χPT and MAχPT compared with the results of the lattice QCD calculations on the m007m050 and m010m050 ensembles. The central values have been chosen to coincide for the larger volume ensembles.

corrections are given by $\Delta m_\pi = (1 \pm 0.3)\Delta m_\pi^{\mathrm{MA}\chi\mathrm{PT}}$, where the central values have been chosen to coincide for the larger volume ensembles. The MAχPT finite-volume contributions appear to not describe the observed volume dependence of m_π, indicating the likely importance of NNLO contributions. In the case of f_π, the volume contributions are in good agreement with the results of the lattice QCD calculations.

C. Strange quark mass effects

The strange quark masses used in the present calculations are not equal to the physical value [89]; the physical staggered strange quark mass was determined to be $bm_s^{\mathrm{phy}} = 0.0350(7)$ and $bm_s^{\mathrm{phy}} = 0.0261(5)$ on the $b \approx 0.125$ fm and $b \approx 0.09$ fm ensembles, respectively [47]. In order to estimate the effects of this small mistuning in the two-flavor expansion, a matching to $SU(3)$ χPT must be performed, where it is found the effects can be absorbed into the NLO LECs [90];

$$\begin{aligned}
\bar{l}_3(m_s, m_s^{\mathrm{phy}}) &= \bar{l}_3(m_s^{\mathrm{phy}}) + \delta\bar{l}_3(m_s, m_s^{\mathrm{phy}}),\\
\delta\bar{l}_3(m_s, m_s^{\mathrm{phy}}) &= -\frac{1}{9}\ln\left(\frac{m_s}{m_s^{\mathrm{phy}}}\right),\\
\bar{l}_4(m_s, m_s^{\mathrm{phy}}) &= \bar{l}_4(m_s^{\mathrm{phy}}) + \delta\bar{l}_4(m_s, m_s^{\mathrm{phy}}),\\
\delta\bar{l}_4(m_s, m_s^{\mathrm{phy}}) &= \frac{1}{4}\ln\left(\frac{m_s}{m_s^{\mathrm{phy}}}\right).
\end{aligned} \tag{22}$$

These lead to mild corrections to $\bar{l}_3$ and $\bar{l}_4$ on both the coarse and fine ensembles,

$$\begin{aligned}
\delta\bar{l}_3(m_s, m_s^{\mathrm{phy}}) &= \begin{cases} -0.040(2), & b \approx 0.125\ \mathrm{fm}, bm_s^{\mathrm{sea}} = 0.05 \\ -0.019(1), & b \approx 0.09\ \mathrm{fm}, bm_s^{\mathrm{sea}} = 0.031; \end{cases}\\
\delta\bar{l}_4(m_s, m_s^{\mathrm{phy}}) &= \begin{cases} 0.089(5), & b \approx 0.125\ \mathrm{fm}, bm_s^{\mathrm{sea}} = 0.05 \\ 0.043(5), & b \approx 0.09\ \mathrm{fm}, bm_s^{\mathrm{sea}} = 0.031. \end{cases}
\end{aligned} \tag{23}$$

These strange quark-mass mistuning effects are negligible compared with the uncertainties of the extracted values for $\bar{l}_3$ and $\bar{l}_4$ (see Sec. IV).

TABLE VII. Parameters used to isolate $m^{\rm res}$ effects. The $L_5 = 16, 24$ calculations were used to tune the quark mass for the $L_5 = 40$ calculation in such a way that the sum $b(m_l + m_l^{\rm res})$ was the same (within ~0.7%) for the $L_5 = 12$ and 40 calculations.

Ensemble	L_5	bm_l	$bm^{\rm res}$	$\frac{m^{\rm res}}{m_l+m^{\rm res}}$	bm_π	bf_π
4096f21b708m0031m031	12	0.0035	0.000428(03)	0.109(1)	$0.10160(22)(^{21}_{24})$	$0.0617(12)(^{10}_{13})$
	16	0.0030	0.000321(11)	0.0987(3)	...	...
	24	0.0030	0.000229(12)	0.071(4)	...	...
	40	0.0038	0.000156(03)	0.039(1)	$0.10328(32)(^{36}_{40})$	$0.0621(09)(^{10}_{13})$

D. Residual chiral symmetry breaking effects

The domain-wall action has residual chiral symmetry breaking due to the finite extent of the fifth dimension, L_5, resulting from the overlap of the chiral modes bound to opposite walls in the fifth dimension. The quantity $m^{\rm res}$ is the leading manifestation of this residual chiral symmetry breaking, and the effective quark mass of the lattice QCD calculation becomes

$$m_q = m_l^{\rm dwf} + m_l^{\rm res}, \tag{24}$$

capturing the dominant effects of the residual chiral symmetry breaking appearing at LO in the chiral Lagrangian. However, it is known that there are subleading effects. Defining the quark mass through Eq. (24) and taking the standard definition of $m^{\rm res}$ as the ratio of two pion to vacuum matrix elements [66]

$$bm^{\rm res} \equiv \frac{\langle 0|J^a_{5q}|\pi\rangle}{\langle 0|J^a_5|\pi\rangle}, \tag{25}$$

where J^a_{5q} and J^a_5 are pseudoscalar densities made, respectively, from quarks in the middle and boundaries of the fifth dimension, the quantity $m^{\rm res} = m^{\rm res}(bm_l, b)$ depends upon the input quark mass and the lattice spacing (see Ref. [9] for a discussion of these effects). Consequently, the chiral Lagrangian receives a simple modification at NLO [91–93]. Following the method of Ref. [94], the modifications to the chiral Lagrangian at NLO are

$$\begin{aligned}\delta\mathcal{L}_{\rm res} = {} & \frac{l_3^{\rm res} + l_4^{\rm res}}{16}\,{\rm tr}(2Bm_q\Sigma + 2Bm_q\Sigma^\dagger) \\ & \times {\rm tr}(2Bm^{\rm res}\Sigma + 2Bm^{\rm res}\Sigma^\dagger) \\ & + \frac{l_4^{\rm res}}{8}\,{\rm tr}(\partial_\mu\Sigma\partial^\mu\Sigma^\dagger)\,{\rm tr}(2Bm^{\rm res}\Sigma + 2Bm^{\rm res}\Sigma^\dagger).\end{aligned} \tag{26}$$

The corrections to m_π and f_π arising from these new terms are

$$\frac{\delta m_\pi^2}{2Bm_q} = -\frac{1}{2}\xi\frac{m^{\rm res}}{m_q}\bar{l}_3^{\rm res} \quad \text{and} \quad \frac{\delta f_\pi}{f} = \xi\frac{m^{\rm res}}{m_q}\bar{l}_4^{\rm res}, \tag{27}$$

with

$$\bar{l}_i^{\rm res} = \frac{32\pi^2}{\gamma_i}\,l_i^{\rm res}, \tag{28}$$

where $\gamma_3 = -1/2$ and $\gamma_4 = 2$ [2]. As with the coefficients l_i^b, these $l_i^{\rm res}$ coefficients are not universal and depend upon the choice of lattice action used.

The new operators in Eq. (26) were found to give the dominant uncertainty in the prediction of the $I = 2\pi\pi$ scattering length at the physical pion mass [25] as the $l_i^{\rm res}$ were unknown. Therefore, for $\pi\pi$ scattering, and for other observables, it is important to determine the $l_i^{\rm res}$, which can be done simply by performing calculations with different values of L_5 on the same ensemble. The fine MILC ensembles, with $b \approx 0.09$ fm, at the lightest quark-mass point were used to perform calculations with $L_5 = 12$ and $L_5 = 40$. The quark mass, defined by Eq. (24), was tuned to be the same for both L_5's, which was achieved to within 0.7% accuracy (giving the same value of m_π^2 up to ~3%). The results of the calculations are presented in Table VII. The values of $l_3^{\rm res}$ and $l_4^{\rm res}$ that are determined by the lattice QCD calculations are presented in Sec. IV.

IV. CHIRAL, CONTINUUM AND VOLUME EXTRAPOLATIONS

The numerical results presented in this work were obtained at several values of the light quark masses and two lattice spacings. To control the discretization effects, it would be ideal to have at least three lattice spacings; however, a third smaller lattice spacing is beyond the scope of this work. To address this limitation, the chiral and continuum extrapolations are performed in two different ways. The first method is to fit the LECs of χPT to the $b \approx 0.125$ fm and $b \approx 0.09$ fm calculations independently. The extracted LECs are then extrapolated to the continuum limit, using the ansatz[2]

$$\lambda(b) = \lambda_0 + \lambda_2\left(\frac{b}{r_1}\right)^2. \tag{29}$$

This analysis is performed at both NLO and NNLO in the chiral expansion. The second method to perform the continuum and chiral extrapolations is to use MAχPT, which leads to determinations of the LECs that are consistent with those obtained with the first method. This lends confidence

[2]The leading discretization corrections in the current formulation of MA lattice QCD scale as $\mathcal{O}(b^2)$.

that the discretization effects are small enough to be captured by the MAχPT formulation.

Before proceeding, it should be noted that the light quark masses are given in lattice units and have not been converted to a continuum regularization scheme. As the product $m_q B$ is renormalization scheme and scale independent, the values of the LEC B, which we determine, have not been properly converted to a continuum regularization scheme. For this reason, we do not provide the results of this quantity.

A. Method 1: χPT and continuum extrapolation

1. NLO SU(2)

The pion masses and decay constants obtained in the lattice QCD calculations on the $b \approx 0.125$ fm and $b \approx 0.09$ fm ensembles are used to determine the LECs at NLO in χPT by independently fitting to the expressions in Eqs. (7) and (8), including the FV corrections in Eqs. (11) and (12). Strange quark-mass effects are included by using Eq. (22), but residual chiral symmetry breaking effects, such as those described by Eq. (27), are not. Both the mass and decay constant depend upon two LECs each, as seen from Eqs. (7) and (8). The uncertainties in the values of ξ and other parameters in Table V are included in our analysis through our Monte Carlo treatment but do not appreciably impact the analysis. Including the larger volume calculations, the complete set of results presented in Table III utilizes six data sets on the $b \approx 0.125$ fm ensembles and three on the $b \approx 0.09$ fm ensembles. For each of the NLO fixed lattice-spacing fits that are presented in Tables VIII and IX, the maximum value of m_l/m_s used in the fit is listed. On the $b \approx 0.125$ fm ensembles, the ratio is in the range $m_l/m_s = 0.14$–0.6, while on the $b \approx 0.09$ fm ensembles the ratio is in the range $m_l/m_s = 0.1$–0.4.[3]

From the quality of fit given in Tables VIII and IX, it is clear that the NLO χPT formula for m_π fails to describe the results of the lattice QCD calculation at either lattice spacing, while the NLO χPT formula for f_π describes the results on the lightest three $b \approx 0.125$ fm ensembles well and describes all the results on the $b \approx 0.09$ fm ensembles.

[3]In addition to giving the χ^2 and the number of degrees of freedom (d.o.f.) in the fit, the Q value, or *confidence of fit*, is also provided,

$$Q \equiv \int_{\chi^2_{\rm min}}^{\infty} d\chi^2 \mathcal{P}(\chi^2, d), \tag{30}$$

where

$$\mathcal{P}(\chi^2, d) = \frac{1}{2^{d/2}\Gamma(d/2)} (\chi^2)^{d/2-1} e^{-\chi^2/2} \tag{31}$$

is the probability distribution function for χ^2 with d degrees of freedom. (The Q value represents the probability that if a random sampling of data were taken from the parent distribution, a larger χ^2 would result.)

TABLE VIII. Results of the fixed lattice-spacing NLO χPT analysis of m_π. Max m_l/m_s denotes the maximum value of the ratio of light quark masses used to perform the analysis.

Max m_l/m_s	$\bar{l}_3$	$b \approx 0.125$ fm $\chi^2_{\rm stat+syst}$	d.o.f.	Q
0.4	5.09(06)(52)	18.1	3	0.00
0.6	4.60(03)(36)	46.6	4	0.00
		$b \approx 0.09$ fm		
m_l/m_s	$\bar{l}_3$	$\chi^2_{\rm stat+syst}$	d.o.f.	Q
0.4	4.05(10)(40)	3.31	1	0.07

TABLE IX. Results of the fixed lattice-spacing NLO χPT analysis of f_π. Max m_l/m_s denotes the maximum value of the ratio of light quark masses used to perform the analysis.

Max m_l/m_s	$r_1 f$	$b \approx 0.125$ fm $\bar{l}_4$	$\chi^2_{\rm stat+syst}$	d.o.f.	Q
0.4	0.2166(10)(40)	4.78(06)(20)	2.35	3	0.50
0.6	0.2109(07)(13)	5.28(03)(10)	15.3	4	0.00
		$b \approx 0.09$ fm			
m_l/m_s	$r_1 f$	$\bar{l}_4$	$\chi^2_{\rm stat+syst}$	d.o.f.	Q
0.4	0.1983(16)(34)	5.48(13)(28)	0.15	1	0.69

Taking the results of the fits with $m_l/m_s \leq 0.4$, a continuum extrapolation of the extracted LECs using Eq. (29) gives

$$\bar{l}_3 = 3.2(0.2)(1.2) \quad \text{and} \quad \bar{l}_4 = 6.3(0.3)(1.1). \tag{32}$$

The NLO χPT determination of $\bar{l}_3$ must be taken with extreme caution (and essentially discarded) as the fit to m_π is poor. This (relatively) large value of $\bar{l}_4$ extracted at NLO is consistent with the JLQCD NLO results using $n_f = 2$ overlap fermions [5].

2. NNLO SU (2)

The pion mass and decay constant at NNLO in χPT, given in Eqs. (14) and (15), depend upon two additional LECs, k_M and k_F, in addition to the appearance of further NLO LECs $\bar{l}_{12} = 7\bar{l}_1 + 8\bar{l}_2$. Both $\bar{l}_1$ and $\bar{l}_2$ are reasonably well determined from $\pi\pi$ scattering [3],

$$\bar{l}_1 = -0.4(6) \quad \text{and} \quad \bar{l}_2 = 4.3(1). \tag{33}$$

To perform the fits at NNLO, these values of $\bar{l}_1$ and $\bar{l}_2$ are used as input. Normal distributions of $\bar{l}_1$ and $\bar{l}_2$ are generated with means and variances given by Eq. (33), which are then used in the fitting process. This allows for a determination of the systematic uncertainty generated by their use as input parameters. In fitting to the results of the

TABLE X. Results of the continuum NNLO χPT analysis of m_π and f_π.

Max m_l/m_s	$r_1 f$	$\bar{l}_3$	$\bar{l}_4$	k_M	k_F	$\chi^2_{\text{stat+syst}}$	d.o.f.	Q
			$b \approx 0.125$ fm					
0.4	0.233(04)(08)	7.95(35)(60)	2.63(37)(67)	29(3)(4)	21(6)(10)	0.53	4	0.74
0.6	0.230(02)(03)	5.83(14)(18)	2.95(14)(24)	14(1)(1)	16(2)(3)	10.0	6	0.12
			$b \approx 0.09$ fm					
	$r_1 f$	$\bar{l}_3$	$\bar{l}_4$	k_M	k_F	$\chi^2_{\text{stat+syst}}$	d.o.f.	Q
0.4	0.203(11)(15)	5.61(67)(73)	4.1(1.1)(1.6)	19(5)(5)	2(17)(25)	0	0	-

calculations on the $b \approx 0.09$ fm ensembles, there are six lattice QCD results, and six fit parameters. The results of this analysis are collected in Table X. The NNLO χPT is found to describe the results of the lattice QCD calculations for both m_π and f_π. Taking the $b \approx 0.125$ fm and $b \approx 0.09$ fm fit and using them to perform a continuum extrapolation,

$$\bar{l}_3 = 3.3(1.4)(1.7) \quad \text{and} \quad \bar{l}_4 = 5.8(2.4)(3.5) \tag{34}$$

are obtained, consistent with those from the NLO analysis. These results must also be treated with caution due to the small number of calculations performed on the $b \approx 0.09$ fm ensembles. In Figs. 8 and 9, one can see the approximate contribution of discretization effects in the values of $\bar{l}_3$ and $\bar{l}_4$.

B. Method 2: Mixed-action χPT

As in the continuum case, the m_π and f_π analyses with MAχPT are decoupled at NLO in the expansion, but the results of the lattice QCD calculations at both lattice spacings can be fit simultaneously. This allows for several choices of fit ranges, which are denoted as A–E in Table XI. The maximum value of m_l/m_s used in the fits from the $b \approx 0.125$ fm and $b \approx 0.09$ fm ensembles are listed in Table XI. As discussed in Sec. III B, the NLO MAχPT volume contributions are assigned a 30% uncertainty as an estimate of NNLO effects. This additional uncertainty is combined in quadrature with the other quoted systematic uncertainties.

TABLE XI. Fit ranges used in the MAχPT analysis. For a given fit, A–E, the maximum value of m_l/m_s (sea-quark masses) is given.

Fit	Max m_l/m_s		
	Coarse $L = 20$	Coarse $L = 24, 28$	Fine
A	0.20	0.20	0.20
B	0.20	0.20	0.40
C	0.40	0.20	0.20
D	0.40	0.20	0.40
E	0.60	0.20	0.40

1. NLO mixed-action χPT

Fits are performed over the ranges listed in Table XI, the results of these analyses are collected in Tables XII and XIII. There are a few observations to make. First, the NLO MAχPT formula is capable of describing the results of the lattice QCD calculations of m_π, unlike the NLO χPT formula. Second, the MAχPT provides a slightly better description of the pion decay constant than of the pion mass. In both cases, the NLO formula is capable of describing the results of the lattice QCD calculations over the full range of quark masses.

As the Q value has a probabilistic interpretation, it is convenient to use it in forming weighted averages of the quantities that have been extracted with multiple fitting procedures and/or different numbers of degrees of freedom. For extractions of a parameter λ from different procedures, each giving λ_i with Q_i, the weighted average

$$\bar{\lambda} = \frac{\sum_i Q_i \lambda_i}{\sum_j Q_j} \tag{35}$$

can be formed.[4] As each of the fits considered in this work, presented in Table XI, includes successively larger quark masses, this averaging will give more weight to the lighter quark-mass values, where χPT is more reliable. Performing this Q-weighted averaging of the results from Tables XII and XIII gives

$$\bar{l}_3[\text{NLO}] = 4.13(20)\left(^{25}_{31}\right), \qquad \bar{l}_4[\text{NLO}] = 6.09(40)\left(^{37}_{45}\right),$$
$$\bar{l}_3^{\text{res}}[\text{NLO}] = 18(5)\left(^{5}_{9}\right), \qquad \bar{l}_4^{\text{res}}[\text{NLO}] = -5(11)\left(^{11}_{12}\right). \tag{36}$$

The value of $\bar{l}_3$ is consistent with the average of all other lattice QCD calculations [12]. However, the value of $\bar{l}_4$ is noticeably higher, but is consistent with that obtained with $N_f = 2$ overlap fermions and a NLO χPT analysis [5]. While the residual chiral symmetry breaking LECs are not

[4]NPLQCD has consistently performed systematic uncertainty analysis by weighting the results of different but equivalent fitting strategies [18–32]. This particular method of Q weighting has also been advocated by the BMW Collaboration [13], for example.

TABLE XII. Results from NLO MAχPT fits to $(r_1 m_\pi)^2/(r_1 m_q)$.

	LECs						
Fit	$\bar{l}_3$	l_3^b	$\bar{l}_3^{\rm res}$	$l_3^{\rm PQ}$	$\chi^2_{\rm stat+syst}$	d.o.f.	Q
A	$4.27(23)(^{36}_{39})$	$-1.23(21)(^{25}_{29})$	$14(6)(^{7}_{8})$	$-0.6(1.6)(^{2.8}_{2.3})$	1.41	2	0.49
B	$4.11(21)(^{29}_{38})$	$-1.09(19)(^{20}_{34})$	$19(5)(^{5}_{9})$	$-2.9(0.9)(^{2.0}_{1.4})$	2.33	3	0.51
C	$4.10(19)(^{21}_{27})$	$-1.16(20)(^{20}_{34})$	$17(6)(^{5}_{9})$	$-1.4(1.5)(^{3.5}_{1.7})$	1.78	3	0.62
D	$4.10(19)(^{21}_{28})$	$-1.09(19)(^{19}_{34})$	$19(5)(^{5}_{9})$	$-2.8(0.8)(^{1.4}_{0.8})$	2.33	4	0.67
E	$4.10(19)(^{21}_{28})$	$-1.13(18)(^{18}_{30})$	$18(5)(^{5}_{8})$	$-2.7(0.7)(^{1.1}_{0.7})$	2.36	5	0.80

TABLE XIII. Results from NLO MAχPT fits to $r_1 f_\pi$.

	LECs							
Fit	$r_1 f$	$\bar{l}_4$	l_4^b	$\bar{l}_4^{\rm res}$	$l_4^{\rm PQ}$	$\chi^2_{\rm stat+syst}$	d.o.f.	Q
A	$0.1847(61)(^{80}_{89})$	$5.80(52)(^{68}_{54})$	$0.6(0.9)(^{1.0}_{1.1})$	$-2(12)(^{15}_{13})$	$-3.8(5.5)(^{8.7}_{7.3})$	0.27	2	0.87
B	$0.1860(20)(^{36}_{89})$	$5.73(42)(^{55}_{39})$	$0.5(0.8)(^{0.8}_{0.9})$	$-1(11)(^{12}_{11})$	$-2.7(2.6)(^{4.4}_{3.2})$	0.28	3	0.96
C	$0.1812(26)(^{55}_{36})$	$6.03(40)(^{38}_{43})$	$0.8(0.8)(^{0.8}_{1.0})$	$-5(12)(^{14}_{11})$	$-6.1(4.4)(^{8.3}_{5.0})$	0.32	3	0.96
D	$0.1841(17)(^{33}_{39})$	$5.99(39)(^{39}_{41})$	$0.4(0.8)(^{0.9}_{0.8})$	$1(11)(^{11}_{12})$	$-0.9(2.4)(^{3.3}_{3.7})$	0.58	4	0.97
E	$0.1797(12)(^{24}_{31})$	$6.10(40)(^{36}_{45})$	$0.9(0.8)(^{0.9}_{0.8})$	$-5(11)(^{11}_{12})$	$-2.9(2.4)(^{2.4}_{4.2})$	3.48	5	0.63

well determined, they will help constrain the analysis of the $I = 2\pi\pi$ scattering length [25].

2. *NLO* MAχPT + NNLO *SU*(2) χPT

While the complete NNLO expressions for the pion mass and decay constant are not available in MAχPT, it is useful to consider the hybrid construction of NLO MAχPT plus NNLO χPT. As in the previous section, the NLO MAχPT volume contributions are assigned a 30% uncertainty. Further, the infinite-volume formulas for the NNLO contributions are used. While the fit values of the NNLO LECs will be polluted by discretization effects, the NLO Gasser-Leutwyler coefficients will be free of these contaminations, and further, their extracted values should be stabilized with the inclusion of these higher order contributions.

The fit functions for m_π and f_π share two LECs; at NNLO, m_π^2 depends upon $\bar{l}_4$ as well as $\bar{l}_3$, and both depend upon $\bar{l}_{12}$; see Eqs. (14) and (15). In principle, a correlated analysis should be performed; however, the correlations only exist at NNLO, and are expected to be insignificant. To capture the effects of the correlations on the central value of $\bar{l}_4$, the extrapolation analysis is performed with a Monte Carlo. Further, as seen in Fig. 7, the NNLO contributions to m_π are insignificant, supporting the above expectation. In order to verify these expectations, a fully correlated fit was performed on a subset of the fits, A–E. The change in the values of the LECs was well contained within the quoted uncertainties. Results of these fits are presented in Table XIV for the various data sets. Taking the Q-weighted average of these results gives

TABLE XIV. Extracted values of the LECs from NLO MAχPT plus NNLO χPT fitting of the lattice QCD results. Data set A has insufficient light quark mass range to constrain the NNLO analysis.

	LECs							
Fit	$r_1 f$	$\bar{l}_3$	$\bar{l}_4$	k_M	k_F	$\chi^2_{\rm stat+syst}$	d.o.f.	Q
A	...	...	...	...	...	...	...	...
B	0.186(9)(13)	$4.48(51)(^{89}_{77})$	$4.83(94)(^{1.4}_{1.3})$	$13(5)(^{8}_{7})$	$-8(17)(^{25}_{24})$	2.22	4	0.69
C	$0.188(7)(^{9}_{11})$	$4.12(30)(^{57}_{71})$	$4.38(55)(^{89}_{65})$	$8(2)(^{4}_{5})$	$1(8)(^{10}_{13})$	2.17	4	0.70
D	$0.193(5)(^{5}_{10})$	$4.00(28)(^{77}_{53})$	$4.10(44)(^{87}_{45})$	$6(2)(^{6}_{3})$	$5(6)(^{7}_{13})$	2.99	6	0.81
E	$0.194(3)(^{5}_{7})$	$3.69(14)(^{18}_{19})$	$4.01(22)(^{36}_{24})$	3(1)(1)	$7(2)(^{3}_{4})$	3.63	8	0.89

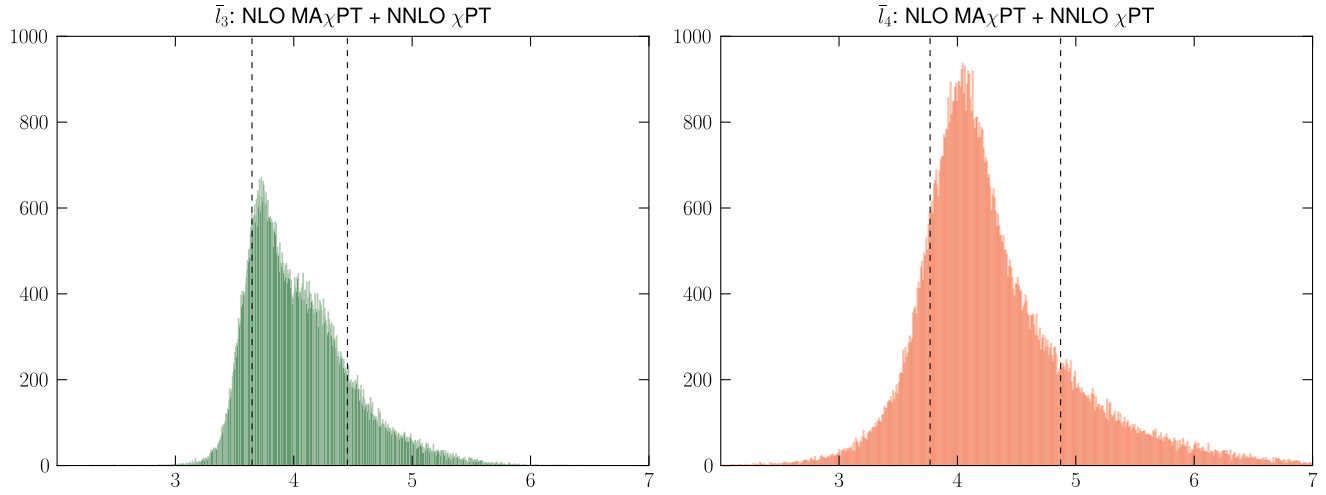

FIG. 5 (color online). $\bar{l}_3$ and $\bar{l}_4$ generated through a Monte Carlo averaging of the fits in Table XIV. The histograms are generated with 10^5 samplings. The vertical dashed lines represent the 16% and 84% quantiles.

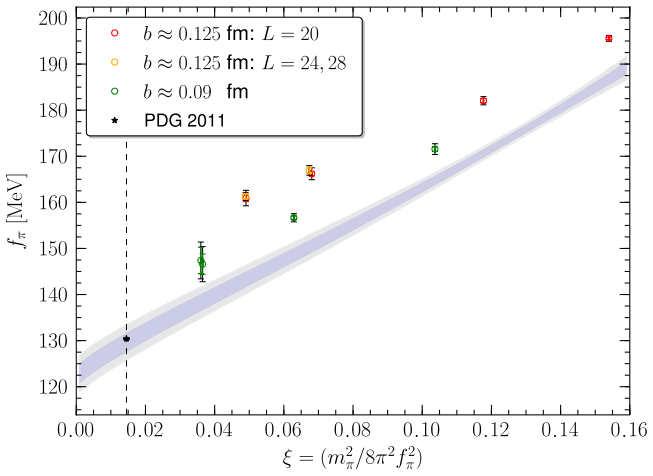

FIG. 6 (color online). The result of NLO MAχPT plus NNLO χPT fit E described in the text, extrapolated to the infinite volume and continuum limits. The star denotes the experimentally determined value of f_{π^+} (not used in the fitting) listed in the Particle Data Group (PDG).

$$\bar{l}_3[\text{NNLO}] = 4.04(40)(^{73}_{55}), \qquad \bar{l}_4[\text{NNLO}] = 4.30(51)(^{84}_{60}),$$
$$\bar{l}_3^{\text{res}}[\text{NNLO}] = 17(5)(^{6}_{10}), \qquad \bar{l}_4^{\text{res}}[\text{NNLO}] = 0(11)(12), \tag{37}$$

with $\bar{l}_3[\text{NNLO}]$ and $\bar{l}_4[\text{NNLO}]$ in good agreement with the averages given in Ref. [12]. At NNLO in the chiral expansion, corrections to the pion decay constant are found to be

$$\frac{f_\pi}{f}[\text{NNLO}] = 1.062(26)(^{42}_{40}). \tag{38}$$

Setting the scale either by using $r_1^{\text{phy}} = 0.311(2)(^{3}_{8})$ fm from the MILC Collaboration to determine f_π^{phy}, or by using the experimental value of f_{π^+} to determine r_1, gives

$$f_\pi^{\text{phy}}[\text{NNLO}] = 128.2(3.6)(^{4.4}_{6.0})(^{1.2}_{3.3})\ \text{MeV} \quad \text{and}$$
$$r_1^{\text{phy}}[\text{NNLO}] = 0.306(9)(^{10}_{14})\ \text{fm}, \tag{39}$$

where the last uncertainty in the postdicted value of f_π comes from MILC's determination of r_1, Eq. (6).

Figure 5 shows Monte Carlo histograms of the extracted values of $\bar{l}_3$ and $\bar{l}_4$ using the Q weights to determine the ratio of samples to draw from each of fits A–E. The result of fit E for f_π, extrapolated to the infinite volume and continuum limits is displayed in Fig. 6. The inner (colored) band represents the 68% statistical confidence interval while the outer (gray) band results from the 68% statistical and systematic uncertainties combined in quadrature. The dashed vertical line is located at ξ^{phy} determined from Eq. (10).

C. Convergence of the $SU(2)$ chiral expansion

With the analyses performed in the previous section in hand, the convergence of the two-flavor chiral expansion can be explored. The resulting NLO and NNLO contributions to the quantities

$$\frac{m_\pi^2}{2Bm_q} - 1 \quad \text{and} \quad \frac{f_\pi}{f} - 1 \tag{40}$$

(both of which vanish in the chiral-limit) are shown in Fig. 7. In both cases (the left and right panels of Fig. 7), it is the continuum limit and infinite-volume limit extrapolations that are displayed. In the case of m_π, the NNLO contributions are negligible over most of the range of ξ

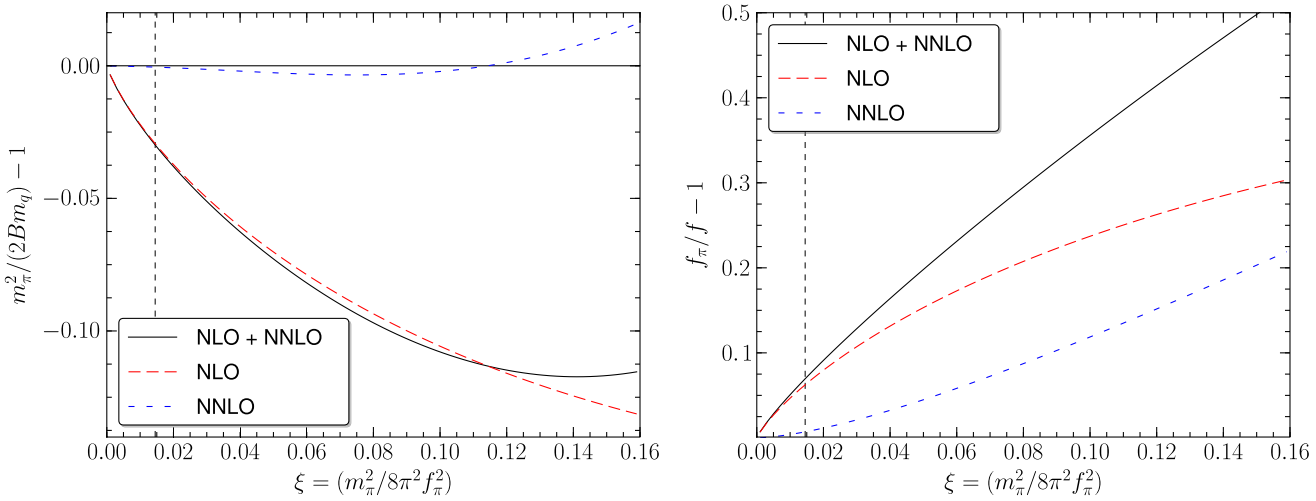

FIG. 7 (color online). The NLO and NNLO contributions to $(m_\pi^2/2Bm_q) - 1$ (left panel) and $(f_\pi/f) - 1$ (right panel). Both of these quantities vanish in the chiral limit. The larger (red) dashed curves are the NLO contributions and the smaller (blue) dashed curves are the NNLO contributions. The solid (black) curve is the entire NLO + NNLO value.

used in our fits. Further, the total corrections to m_π are small, being less than ~15% over the full range of quark masses. In contrast, the corrections to f_π become substantial at the heavier pion masses, exceeding ~50% at the heaviest mass considered. Further, at the modest value of $\xi \gtrsim 0.08$ the NNLO corrections become significant compared to the NLO corrections.

In the left panel of Fig. 8, the determination of $\bar{l}_3$ is shown. The results of the fixed lattice spacing χPT analysis from Sec. IV A 2 is displayed, as well as the continuum extrapolated value. Also shown are the values extracted from MAχPT at NLO, and from NLO MAχPT supplemented with continuum NNLO χPT, as discussed in Secs. IV B 1 and IV B 2, respectively. The results of the MAχPT analyses are consistent with the continuum extrapolated results, but with smaller uncertainties. This is not surprising as the mixed-action framework allows a simultaneous treatment of calculational results from multiple lattice spacings. This consistency lends confidence in the entire analysis. In the right panel of Fig. 8, the extraction is compared to the original estimates by Gasser and Leutwyler [2] as well as to the recent lattice QCD average [12]. In Fig. 9, the analogous results for $\bar{l}_4$ are displayed, although Ref. [12] does not provide an average value (citing insufficient reporting of the associated systematic uncertainties).

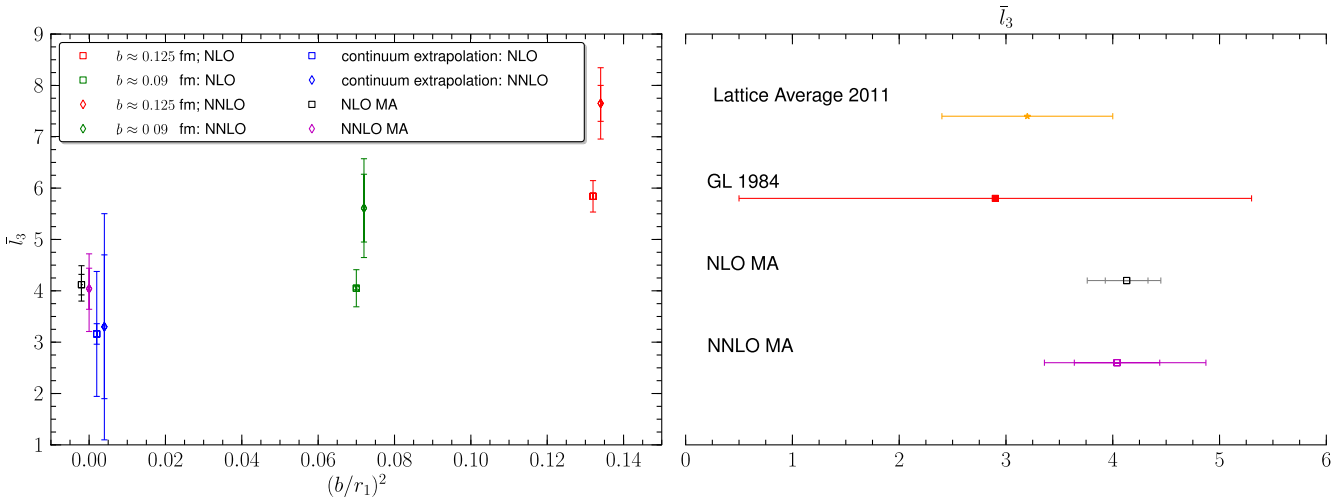

FIG. 8 (color online). The present determination of $\bar{l}_3$ (left panel), and its comparison to the lattice QCD average value [12] and phenomenological results (right panel). Some of the $\bar{l}_3$ results in the left panel have been given small offsets in $(b/r_1)^2$ for presentations reasons.

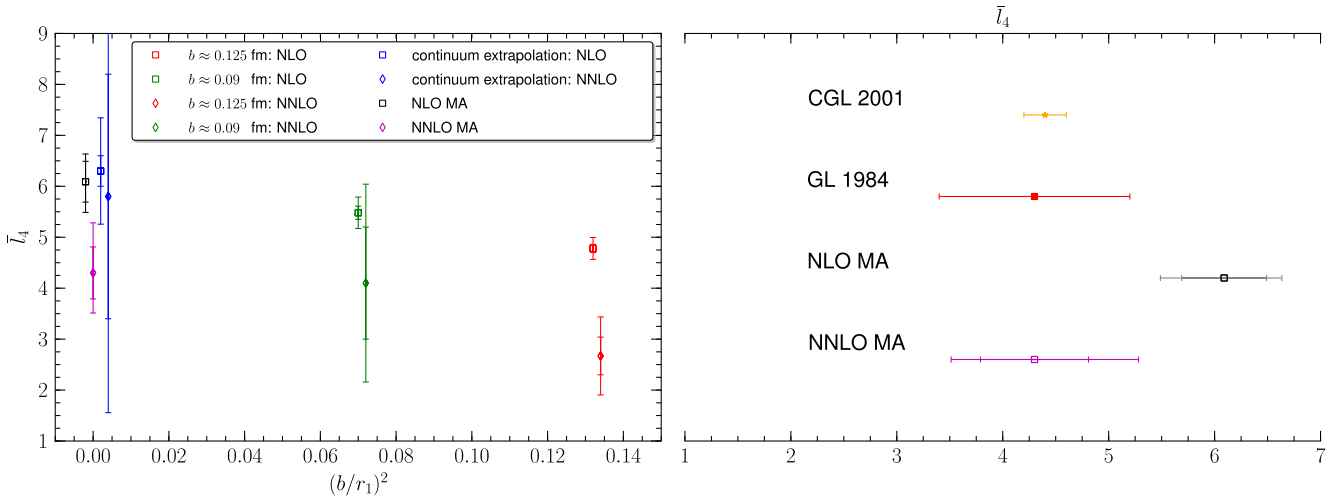

FIG. 9 (color online). The present determination of $\bar{l}_4$ (left panel), and its comparison with phenomenological results (right panel). (Reference [12] does not currently provide a lattice QCD average value for this quantity.) Some of the $\bar{l}_4$ results in the left panel have been given small offsets in $(b/r_1)^2$ for presentations reasons. CGL 2001 refers to Ref. [3].

V. RESULTS AND DISCUSSION

We have performed precision calculations of the pion mass and the pion decay constant with mixed-action lattice QCD. Calculations using domain-wall valence quarks and staggered sea quarks were performed on a number of ensembles of MILC gauge-field configurations at different light quark masses, two lattice spacings, different volumes and different extents of the fifth dimension. Using the two lattice spacings and the multiple light quark masses, the results of these calculations were extrapolated to the continuum, to infinite volume and to the physical pion mass. Ideally, continuum extrapolations would be performed with more than two lattice spacings. While this is not possible with the present numerical results, the two methods used to quantify uncertainties associated with the continuum extrapolation from the two lattice spacings used in this work are found to give the same results within uncertainties. One method involved using two-flavor χPT to extract the LECs, which implicitly include lattice-spacing artifacts. LECs calculated at two different lattice spacings were then extrapolated to the continuum. It is found that NLO χPT fails to describe the results of the Lattice calculations of m_π, while NNLO χPT appears to be consistent with them. The second method was to use MAχPT where the lattice-spacing artifacts are explicit, and the extracted LECs are those of the continuum, up to higher order contributions. A hybrid analysis was motivated to be sufficient, where the mixed-action NLO contributions were combined with continuum NNLO contributions to provide reliable extractions of the LECs. These analyses have provided determinations of the Gasser-Leutwyler coefficients $\bar{l}_3$ and $\bar{l}_4$,

$$\bar{l}_3 = 4.04(40)(^{73}_{55}) \quad \text{and} \quad \bar{l}_4 = 4.30(51)(^{84}_{60}). \tag{41}$$

These values are consistent with the (lattice) averaged values reported in Ref. [12]. Our analysis also provides

$$\frac{f_\pi}{f} = 1.062(26)(^{42}_{40}), \tag{42}$$

which is to be compared to the lattice averaged value of $f_\pi/f = 1.073(15)$. Combined with the experimental value for $f_\pi^{\text{phy}} = 130.4$ MeV, a value of $f = 122.8(3.0) \times (^{4.6}_{4.8})$ MeV is found (we have not accounted for explicit isospin breaking effects, but these are expected to be small). In Table XV, the present results are compared with those of the most recent calculations from other lattice collaborations. Further, the extrapolated value of $r_1 f_\pi$ and the experimentally measured value of f_{π^+} provide a determination of the physical scale r_1,

$$r_1 = 0.306(9)(^{10}_{14}) \text{ fm}, \tag{43}$$

which is to be compared with the MILC determination (on the same ensembles) of $r_1 = 0.311(2)(^{3}_{8})$ fm. It is interesting to note that, despite greatly enhanced statistics on the same ensembles of MILC gauge-field configurations, the uncertainty that we have obtained in the calculation of f_π is somewhat larger than that obtained in Ref. [17].

The systematics in the calculations arising from the finite lattice volume and from residual chiral symmetry breaking due to the finite fifth-dimensional extent of the domain-wall action have been explored and quantified. Previously, residual chiral symmetry breaking contributions were identified to be the dominant source of uncertainty in lattice QCD predictions of the $I = 2\pi\pi$ scattering length [25]. While the present analysis has not been able to precisely determine these effects, the analysis resulted in constraints on the size of these contributions,

TABLE XV. Comparison with most recent results from various lattice collaborations.

Collaboration	Reference	N_f	f_π/f	$\bar{l}_3$	$\bar{l}_4$
MILC 10 [$SU(3)$]	[11]	$2+1$	1.06(5)	3.18(50)(89)	4.29(21)(82)
MILC 10A [$SU(2)$]	[10]	$2+1$	1.05(1)	$2.85(81)(^{37}_{92})$	$3.98(32)(^{51}_{28})$
RBC/UKQCD 10A	[9]	$2+1$	$\cdots$	2.57(18)	3.83(09)
ETM 10	[8]	$2+1+1$	1.076(2)(2)	3.70(07)(26)	4.67(03)(10)
ETM 09C	[7]	2	$1.0755(6)(^{08}_{94})$	$3.50(9)(^{09}_{30})$	$4.66(4)(^{04}_{33})$
PACS-CS 08 [$SU(3)$]	[6]	$2+1$	1.062(8)	3.47(11)	4.21(11)
PACS-CS 08 [$SU(2)$]	[6]	$2+1$	1.060(7)	3.14(23)	4.04(19)
JLQCD/TWQCD 08A	[5]	2	1.17(4)	$3.38(40)(24)(^{31}_{0})$	$4.12(35)(30)(^{31}_{0})$
RBC/UKQCD 08	[4]	$2+1$	1.080(8)	3.13(33)(24)	4.43(14)(77)
FLAG Avg.	[12]	–	1.073(15)	3.2(8)	–
NPLQCD [this work]		$2+1$	$1.062(26)(^{42}_{40})$	$4.04(40)(^{73}_{55})$	$4.30(51)(^{84}_{60})$

TABLE XVI. Error budget for current work expressed as relative uncertainties.

Quantity	Total uncertainty	Statistical uncertainty	Chiral extrapolation	Continuum extrapolation	Volume extrapolation	$m^{\rm res}$	$m_s^{\rm tune}$
$\bar{l}_3$	19%	10%	15%	5%	0%	2.7%	0%
$\bar{l}_4$	21%	7%	19%	4%	0%	4%	0%
f_π/f	4.6%	2.4%	3.9%	0%	0%	0%	0%

$$\bar{l}_3^{\rm res} = 17(5)(^{6}_{10}), \qquad \bar{l}_4^{\rm res} = 0(11)(12), \tag{44}$$

which in turn can be used to reduce the uncertainties in the $I = 2\pi\pi$ scattering length predictions.

The predicted NLO mixed-action finite-volume contributions to the pion mass appear to be incompatible with the results of the lattice QCD calculations, suggesting the importance of higher orders in the MAχPT expansion. A 30% systematic uncertainty is assigned to the NLO finite-volume contributions to account for NNLO effects, leading to a consistent description of the results.

In Table XVI the contributions to the total uncertainty from the various systematics are displayed. While the discretization and residual chiral symmetry breaking effects have some impact on the determination of the LECs, it is clear from this summary table that the dominant uncertainty is due to the chiral extrapolation. Having further numerical results at lighter pion masses is the single most important systematic to address to improve upon the present work.

In conclusion, we have found that a careful two-flavor low-energy effective field theory analysis of the lattice QCD calculations of the pion mass and its decay constant can reliably determine the NLO Gasser-Leutwyler coefficients, $\bar{l}_3$ and $\bar{l}_4$, which are found to be in good agreement with the average of other determinations. In particular, mixed-action chiral perturbation theory which includes lattice-spacing artifacts explicitly, provides a reliable framework with which to perform chiral extrapolations of m_π and f_π to the physical light quark masses, and to determine $\bar{l}_3$ and $\bar{l}_4$.

ACKNOWLEDGMENTS

We would to thank the LHP Collaboration for their light quark propagators computed on the $b \approx 0.125$ fm from MILC as well as those extrapolated to the physical values of the light quark masses. We thank G. Colangelo for valuable conversations and R. Edwards and B. Joo for developing QDP++ and CHROMA [95]. We would also like to thank H.-W. Lin for comments on the manuscript. We acknowledge computational support from the USQCD SciDAC project, National Energy Research Scientific Computing Center (NERSC, Office of Science of the DOE, Grant No. DE-AC02-05CH11231), the UW HYAK facility, Centro Nacional de Supercomputación (Barcelona, Spain), LLNL, the Argonne Leadership Computing Facility at Argonne National Laboratory (Office of Science of the DOE, under Contract No. DE-AC02-06CH11357), and the NSF through Teragrid resources provided by TACC and NICS under Grant No. TG-MCA06N025. S. R. B. was supported in part by the NSF CAREER Grant No. PHY-0645570. The Albert Einstein Center for Fundamental Physics is supported by the Innovations- und Kooperationsprojekt C-13 of the Schweizerische Universitätskonferenz SUK/CRUS.

The work of A. P. is supported by the Contract No. FIS2008-01661 from MEC (Spain) and FEDER and from the RTN Flavianet MRTN-CT-2006-035482 (EU). M. J. S. is supported in part by the DOE Grant No. DE-FG03-97ER4014. W. D. and K. O. were supported in part by DOE Grants No. DE-AC05-06OR23177 (JSA) and No. DE-FG02-04ER41302. W. D. was also supported by DOE OJI Grant No. DE-SC0001784 and Jeffress Memorial Trust, Grant No. J-968. K. O. was also supported in part by NSF Grant No. CCF-0728915 and DOE OJI Grant No. DE-FG02-07ER41527. A. T. was supported by NSF Grant No. PHY-0555234 and DOE Grant No. DE-FC02-06ER41443. The work of T. L. was performed under the auspices of the U.S. Department of Energy by LLNL under Contract No. DE-AC52-07NA27344. The work of A. W. L. was supported in part by the Director, Office of Energy Research, Office of High Energy and Nuclear Physics, Divisions of Nuclear Physics, of the U.S. DOE under Contract No. DE-AC02-05CH11231.

[1] S. Weinberg, Physica (Amsterdam) **96A**, 327 (1979).
[2] J. Gasser and H. Leutwyler, Ann. Phys. (N.Y.) **158**, 142 (1984).
[3] G. Colangelo, J. Gasser, and H. Leutwyler, Nucl. Phys. **B603**, 125 (2001).
[4] C. Allton *et al.* (RBC and UKQCD Collaborations), Phys. Rev. D **78**, 114509 (2008).
[5] J. Noaki *et al.* (JLQCD and TWQCD Collaborations), Phys. Rev. Lett. **101**, 202004 (2008).
[6] S. Aoki *et al.* (PACS-CS Collaboration), Phys. Rev. D **79**, 034503 (2009).
[7] R. Baron *et al.* (ETM Collaboration), J. High Energy Phys. 08 (2010) 097.
[8] R. Baron *et al.*, J. High Energy Phys. 06 (2010) 111.
[9] Y. Aoki *et al.* (RBC and UKQCD Collaborations), Phys. Rev. D **83**, 074508 (2011).
[10] A. Bazavov *et al.*, Proc. Sci., LATTICE2010 (2010) 083.
[11] A. Bazavov *et al.* (MILC Collaboration), Proc. Sci., LATTICE2010 (2010) 074.
[12] G. Colangelo *et al.*, Eur. Phys. J. C **71**, 1695 (2011).
[13] S. Dürr *et al.* (BMW Collaboration), Science **322**, 1224 (2008).
[14] S. Aoki *et al.* (PACS-CS Collaboration), Phys. Rev. D **81**, 074503 (2010).
[15] S. Dürr, Z. Fodor, C. Hoelbling, S. D. Katz, S. Krieg, T. Kurth, L. Lellouch, T. Lippert, K. K. Szabó, and G. Vulvert (BMW Collaboration), Phys. Lett. B **701**, 265 (2011).
[16] S. Dürr, Z. Fodor, C. Hoelbling, S. D. Katz, S. Krieg, T. Kurth, L. Lellouch, T. Lippert, K. K. Szabó, and G. Vulvert (BMW Collaboration), J. High Energy Phys. 08 (2011) 148.
[17] C. Aubin, J. Laiho, and R. S. Van de Water, Proc. Sci., LATTICE2008 (2008) 105 [arXiv:0810.4328].
[18] S. R. Beane, P. F. Bedaque, K. Orginos, and M. J. Savage (NPLQCD Collaboration), Phys. Rev. D **73**, 054503 (2006).
[19] S. R. Beane, P. F. Bedaque, K. Orginos, and M. J. Savage, Phys. Rev. Lett. **97**, 012001 (2006).
[20] S. R. Beane, K. Orginos, and M. J. Savage (NPLQCD Collaboration), Phys. Lett. B **654**, 20 (2007).
[21] S. R. Beane, K. Orginos, and M. J. Savage (NPLQCD Collaboration), Nucl. Phys. **B768**, 38 (2007).
[22] S. R. Beane, P. F. Bedaque, K. Orginos, and M. J. Savage (NPLQCD Collaboration), Phys. Rev. D **75**, 094501 (2007).
[23] S. R. Beane, P. F. Bedaque, T. C Luu, K. Orginos, E. Pallante, A. Parreño, and M. J. Savage (NPLQCD Collaboration), Phys. Rev. D **74**, 114503 (2006).
[24] S. R. Beane, P. F. Bedaque, T. C. Luu, K. Orginos, E. Pallante, A. Parreño, and M. J. Savage (NPLQCD Collaboration), Nucl. Phys. **794A**, 62 (2007).
[25] S. R. Beane, T. C. Luu, K. Orginos, A. Parreño, M. J. Savage, A. Torok, and A. Walker-Loud (NPLQCD Collaboration), Phys. Rev. D **77**, 014505 (2008).
[26] S. R. Beane, T. C. Luu, K, Orginos, A. Parreño, M. J. Savage, A. Torok, and A. Walker-Loud (NPLQCD Collaboration), Phys. Rev. D **77**, 094507 (2008).
[27] S. R. Beane, W. Detmold, T. C. Luu, K. Orginos, M. J. Savage, and A. Torok (NPLQCD Collaboration), Phys. Rev. Lett. **100**, 082004 (2008).
[28] W. Detmold, M. J. Savage, A. Torok, S. R. Beane, T, C. Luu, K. Orginos, and A. Parreño (NPLQCD Collaboration), Phys. Rev. D **78**, 014507 (2008).
[29] S. R. Beane, K. Orginos, and M. J. Savage (NPLQCD Collaboration), Int. J. Mod. Phys. E **17**, 1157 (2008).
[30] W. Detmold, K. Orginos, M. J. Savage, and A. Walker-Loud (NPLQCD Collaboration), Phys. Rev. D **78**, 054514 (2008).
[31] W. Detmold and M. J. Savage (NPLQCD Collaboration), Phys. Rev. Lett. **102**, 032004 (2009).
[32] A. Torok, S. R. Beane, W. Detmold, T. C. Luu, K. Orginos, A. Parreño, M. J. Savage, and A. Walker-Loud (NPLQCD Collaboration), Phys. Rev. D **81**, 074506 (2010).
[33] D. B. Renner, W. Schroers, R. Edwards, G. T. Fleming, Ph. Hägler, J. W. Negele, K. Orginos, A. V. Pochinski, and D. Richards (LHPC), Nucl. Phys. B, Proc. Suppl. **140**, 255 (2005).
[34] R. G. Edwards *et al.* (LHPC), Proc. Sci., LAT2005 (2006) 056 [arXiv:hep-lat/0509185].
[35] R. G. Edwards, G. Fleming, Ph. Hägler, J. Negele, K. Orginos, A. Pochinsky, D. Renner, D. Richards, and W. Schroers (LHPC), Phys. Rev. Lett. **96**, 052001 (2006).
[36] P. Hägler *et al.* (LHPC), Phys. Rev. D **77**, 094502 (2008).
[37] A. Walker-Loud *et al.*, Phys. Rev. D **79**, 054502 (2009).
[38] J. D. Bratt *et al.* (LHPC), Phys. Rev. D **82**, 094502 (2010).
[39] D. B. Kaplan, Phys. Lett. B **288**, 342 (1992).
[40] Y. Shamir, Phys. Lett. B **305**, 357 (1993).
[41] Y. Shamir, Nucl. Phys. **B406**, 90 (1993).
[42] Y. Shamir, Phys. Rev. D **59**, 054506 (1999).

[43] V. Furman and Y. Shamir, Nucl. Phys. **B439**, 54 (1995).
[44] K. Orginos and D. Toussaint, Phys. Rev. D **59**, 014501 (1998).
[45] K. Orginos, D. Toussaint, and R. L. Sugar (MILC Collaboration), Phys. Rev. D **60**, 054503 (1999).
[46] C. W. Bernard, T. Burch, K. Orginos, D. Toussaint, T. DeGrand, Ca. DeTar, S. Datta, S. Gottlieb, U. Heller, and R. Sugar, Phys. Rev. D **64**, 054506 (2001).
[47] A. Bazavov *et al.*, Rev. Mod. Phys. **82**, 1349 (2010).
[48] A. Hasenfratz and F. Knechtli, Phys. Rev. D **64**, 034504 (2001).
[49] T. A. DeGrand, A. Hasenfratz, and T. G. Kovacs, Phys. Rev. D **67**, 054501 (2003).
[50] T. A. DeGrand, Phys. Rev. D **69**, 074024 (2004).
[51] S. Dürr, C. Hoelbling, and U. Wenger, Phys. Rev. D **70**, 094502 (2004).
[52] J.-W. Chen, D. O'Connell, R. S. Van de Water, and A. Walker-Loud, Phys. Rev. D **73**, 074510 (2006).
[53] J.-W. Chen, D. O'Connell, and A. Walker-Loud, Phys. Rev. D **75**, 054501 (2007).
[54] J.-W. Chen, D. O'Connell, and A. Walker-Loud, J. High Energy Phys. 04 (2009) 090.
[55] E. E. Jenkins and R. F. Lebed, Phys. Rev. D **52**, 282 (1995).
[56] E. E. Jenkins, A. V. Manohar, J. W. Negele, and A. Walker-Loud, Phys. Rev. D **81**, 014502 (2010).
[57] H.-W. Lin, S. D. Cohen, N. Mathur, and K. Orginos, Phys. Rev. D **80**, 054027 (2009).
[58] L. Liu, H.-W. Lin, K. Orginos, and A. Walker-Loud, Phys. Rev. D **81**, 094505 (2010).
[59] H.-W. Lin and K. Orginos, Phys. Rev. D **79**, 034507 (2009).
[60] H.-W. Lin and K. Orginos, Phys. Rev. D **79**, 074507 (2009).
[61] C. Aubin, J. Laiho, and R. S. Van de Water, Phys. Rev. D **81**, 014507 (2010).
[62] C. Aubin, J. Laiho, and R. S. Van de Water, Phys. Rev. D **77**, 114501 (2008).
[63] S. Prelovsek, Phys. Rev. D **73**, 014506 (2006).
[64] A. Frommer, B. Nockel, S. Gusken, T. Lippert, and K. Schilling, Int. J. Mod. Phys. C **6**, 627 (1995).
[65] A. V. Pochinsky, Ph.D. thesis, MIT, 1997.
[66] T. Blum *et al.*, Phys. Rev. D **69**, 074502 (2004).
[67] K. Orginos and A. Walker-Loud, Phys. Rev. D **77**, 094505 (2008).
[68] Y. Aoki *et al.* (RBC and UKQCD Collaborations), Phys. Rev. D **84**, 014503 (2011).
[69] S. Aoki, M. Fukugita, S. Hashimoto, Y. Iwasaki, K. Kanaya, Y. Kuramashi, H. Mino, M. Okawa, A. Ukawa, and T. Yoshié (JLQCD Collaboration), Nucl. Phys. B, Proc. Suppl. **47**, 354 (1996).
[70] S. R. Beane, W. Detmold, T. C. Luu, K. Orginos, A. Parreño, M. Savage, A. Torok, and A. Walker-Loud, Phys. Rev. D **79**, 114502 (2009).
[71] S. R. Beane, W. Detmold, T. C. Luu, K. Orginos, A. Parreño, M. Savage, A. Torok, and A. Walker-Loud, Phys. Rev. D **80**, 074501 (2009).
[72] S. R. Beane, W. Detmold, H.-W. Lin, T. C. Luu, K. Orginos, M. J. Savage, A. Torok, and A. Walker-Loud (NPLQCD Collaboration), Phys. Rev. D **81**, 054505 (2010).
[73] S. R. Beane, E. Chang, W. Detmold, H. W. Lin, T. C. Luu, K. Orginos, A. Parreño, M. J. Savage, A. Torok, and A. Walker-Loud, Phys. Rev. D **84**, 014507 (2011).
[74] R. Sommer, Nucl. Phys. **B411**, 839 (1994).
[75] J. Gasser and H. Leutwyler, Phys. Lett. B **184**, 83 (1987).
[76] G. Colangelo and S. Dürr, Eur. Phys. J. C **33**, 543 (2004).
[77] J. Bijnens, G. Colangelo, and P. Talavera, J. High Energy Phys. 05 (1998) 014.
[78] O. Bär, G. Rupak, and N. Shoresh, Phys. Rev. D **67**, 114505 (2003).
[79] O. Bär, G. Rupak, and N. Shoresh, Phys. Rev. D **70**, 034508 (2004).
[80] O. Bär, C. Bernard, G. Rupak, and N. Shoresh, Phys. Rev. D **72**, 054502 (2005).
[81] M. Golterman, T. Izubuchi, and Y. Shamir, Phys. Rev. D **71**, 114508 (2005).
[82] B. C. Tiburzi, Phys. Rev. D **72**, 094501 (2005).
[83] C. Aubin, J. Laiho, and R. S. Van de Water, Phys. Rev. D **75**, 034502 (2007).
[84] F.-J. Jiang, arXiv:hep-lat/0703012.
[85] J.-W. Chen, M. Golterman, D. O'Connell, and A. Walker-Loud, Phys. Rev. D **79**, 117502 (2009).
[86] P. H. Ginsparg and K. G. Wilson, Phys. Rev. D **25**, 2649 (1982).
[87] S. R. Sharpe, Phys. Rev. D **56**, 7052 (1997).
[88] G. Colangelo, S. Dürr, and C. Haefeli, Nucl. Phys. **B721**, 136 (2005).
[89] C. Aubin *et al.*, Phys. Rev. D **70**, 031504 (2004).
[90] J. Gasser and H. Leutwyler, Nucl. Phys. **B250**, 465 (1985).
[91] T. Blum *et al.*, Phys. Rev. D **68**, 114506 (2003).
[92] M. Golterman, Y. Shamir, and B. Svetitsky, Phys. Rev. D **72**, 034501 (2005).
[93] S. R. Sharpe, arXiv:0706.0218.
[94] S. R. Sharpe and R. L. Singleton, Jr., Phys. Rev. D **58**, 074501 (1998).
[95] R. G. Edwards and B. Joo (SciDAC Collaboration), Nucl. Phys. B, Proc. Suppl. **140**, 832 (2005).